

Review

# Ranges of Physical Parameters and Geochemical Features of Mineralizing Fluids at Porphyry Deposits of Various Types of the Cu–Mo–Au System: Evidence from Fluid Inclusions Data

Vsevolod Yu. Prokofiev <sup>1,\*</sup>  and Vladimir B. Naumov <sup>2</sup>

<sup>1</sup> The Institute of the Geology of Ore Deposits, Petrography, Mineralogy, and Geochemistry (IGEM), Russian Academy of Sciences, 109017 Moscow, Russia

<sup>2</sup> Vernadsky Institute of Geochemistry and Analytical Chemistry, Russian Academy of Sciences, 119991 Moscow, Russia; naumov@geokhi.ru

\* Correspondence: vpr2004@rambler.ru

**Abstract:** The paper reviews and summarizes data on the physicochemical parameters and chemical features of mineralizing fluids at porphyry deposits of the Cu–Mo–Au system. The calculated average values and ranges of parameters of the fluids in mineral-hosted fluid inclusions at porphyry deposits are as follows: temperature 90–957 °C, average 388 °C; salinity 0.1–88.0 wt % equiv. NaCl, average 29.4 wt % equiv. NaCl; and density 0.38–1.85 g/cm<sup>3</sup>, average 0.93 g/cm<sup>3</sup>. The highest average temperature and the highest maximum homogenization temperatures of the fluids were detected at deposits of the Cu (Au) type, with both values systematically decreasing with the transition to the Cu, Mo (Au), and then to Mo and Au types of porphyry deposits. The situations with the average and maximum salinity values of the fluids and their density are analogous. The data in the literature on the concentrations of some elements are still insufficient to reliably characterize variations in these concentrations at all of the discussed types of porphyry deposits. The highest Cu and Fe concentrations were found in the highest temperature fluids at deposits of the Cu (Au) type. The maximum Mo concentrations were detected in fluids at porphyry Mo deposits, and the highest Ag concentrations occurred at porphyry Au deposits. The chemical composition of the mineralizing fluids is, thus, strongly correlated with the types of the porphyry deposits. The hypothesis is discussed: the geochemical specifics of mineralizing fluids at various types of porphyry deposits of the Cu–Mo–Au system are related to the depths at which fluid separated from the magmatic melt. A scenario is proposed for the separation of mineralizing fluids from granite melt at various depths for fluids that form different types of porphyry deposits.

**Keywords:** porphyry deposits; copper; molybdenum; gold; fluid inclusions



**Citation:** Prokofiev, V.Y.; Naumov, V.B. Ranges of Physical Parameters and Geochemical Features of Mineralizing Fluids at Porphyry Deposits of Various Types of the Cu–Mo–Au System: Evidence from Fluid Inclusions Data. *Minerals* **2022**, *12*, 529. <https://doi.org/10.3390/min12050529>

Academic Editors: Yong Lai and Liqiang Yang

Received: 5 February 2022

Accepted: 20 April 2022

Published: 24 April 2022

**Publisher's Note:** MDPI stays neutral with regard to jurisdictional claims in published maps and institutional affiliations.



**Copyright:** © 2022 by the authors. Licensee MDPI, Basel, Switzerland. This article is an open access article distributed under the terms and conditions of the Creative Commons Attribution (CC BY) license (<https://creativecommons.org/licenses/by/4.0/>).

## 1. Introduction

The porphyry type of hydrothermal mineral deposits is of paramount economic importance because deposits of this type host much of the world's reserves of Cu, Mo, and Re, as well as much Re and remarkable reserves of critical elements such as Ag, Pd, Te, Se, Bi, Zn, and Pb (e.g., [1–4]). Porphyry deposits are conventionally classified into mineralogical–geochemical types according to their dominant valuable components, e.g., [3]. The most economically important porphyry-type deposits are those of the Cu (Au), Cu–Mo (Au), Mo, and Au types.

Porphyry deposits have been studied for a long time, and their features have been much discussed in many reviews, e.g., [5]. Detailed reviews were published on the geology and geotectonic settings of porphyry deposits, zoning of the wall-rock metasomatites, and spatiotemporal relations between the ore mineralization and magmatism in porphyry systems, e.g., [3,4,6–9].

Porphyry deposits contain large reserves of ores with low Cu, Mo, and Au concentrations and are genetically linked to the emplacements and crystallization of melts ranging from diorite to granite in composition. Magma bodies that generate porphyry mineralization are usually constrained to plate margins, e.g., [1–4,7,8]. Porphyry deposits are usually zonal [10] and are stockworks of disseminated and stringer accumulations of sulfides and oxides hosted in large (up to 10 km<sup>3</sup>) volumes of hydrothermally altered rocks, which were produced by the large-scale circulation of hydrothermal fluids at upper crustal levels [2–4,11–14]. Porphyry deposits were found in continental magmatic belts worldwide, showing evidence of spatiotemporal and genetic relations to hypabyssal porphyritic diorite and granodiorite intrusions, which were produced by water-rich magmas.

According to the orthomagmatic model [4,10,15,16], porphyry copper mineralized magmas are usually emplaced into upper crustal levels (at depths of approximately 5–10 km). The gradually cooling melts approach their saturation with volatile components [17,18]. As soon as the melt reaches its saturation with volatiles, a phase of aqueous magmatic fluid (whose salinity is not high) is separated from the melt [17,18], and some elements (including sulfur, chlorine, copper, and some other metals) are, therewith, transferred from the melt into the aqueous phase to form mineralized aqueous magmatic fluid [3,19–31]. Magmatic fluid ascends along fractures and cracks into the already-solid parts of the intrusions, alters host rocks, and comes, due to the pressure decrease, to the field of two-phase equilibrium, in which pressure is lower than 1300 bar (i.e., the region of ore deposition). In this region, the fluid exsolves (heterogenizes) into two phases: chloride brine and a low-density aqueous fluid [32,33]. The heterogenization of the fluid triggers the onset of ore deposition. The fluids then continue cooling, interacting with rocks and diluted meteoric waters, and depositing ore and gangue minerals [4,12,14,16]. Relics of the mineralizing fluids are captured as fluid inclusions, which can provide a record of the evolution of the parameters and composition of the fluids with time [34]. Many researchers have demonstrated that parameters of mineral-hosted fluid inclusions in porphyry hydrothermal systems systematically vary in space and with time, e.g., [26,31,34–39]. A model developed for H<sub>2</sub>O–NaCl fluid is able to realistically describe the distributions of various types of fluid inclusions (halite-bearing brine inclusions, gas inclusions, and liquid-rich two-phase inclusions) over the volumes of porphyry copper deposits [40]. Assemblages of brine and gas fluid inclusions mark domains with high-grade ores. It is important to specify that the fluid inclusion assemblage (FIA) is usually defined as the most finely discriminated group of cogenetic fluid inclusions occupying an individual petrographic feature (e.g., crystal growth-zone or healed fracture), as is unambiguously recognizable by microscopic methods. This model is able to predict the composition and parameters of fluid inclusions captured by minerals when porphyry fluid–magma systems spatiotemporally develop, which enables one to utilize these data for various practical purposes. Although porphyry deposits were studied in much detail, it is still interesting to correlate current understandings of their genesis with the available data on mineral-hosted fluid inclusions in porphyry Cu–Mo–Au systems.

It is pertinent to mention the following reviews of fluid inclusions in the minerals of porphyry systems, e.g., [5,26,34,38,41–45]. Some reviews were devoted to the parameters and composition of fluid inclusions in minerals from porphyry deposits, e.g., [31,46,47]. Fluid inclusions hosted in minerals at porphyry deposits are still actively studied, and extensive newly acquired data were published after the aforementioned reviews. Differences between the physicochemical parameters of fluids that produced all of the four types of porphyry deposits in the Cu–Mo–Au system still have not been adequately analyzed in the literature, likely because of the very broad variations in the homogenization temperature and salinity of the fluid inclusions.

This paper reviews the published data on fluid inclusions (obtained by conventional microthermometric methods and by analyzing the chemical composition of individual fluid inclusions by the technique of high spatial resolution) to evaluate the overall ranges of the physicochemical parameters and identify general trends in the variations in the chemical

composition of mineralizing fluids in porphyry Cu–Mo–Au systems. It is also interesting to understand the differences in the parameters and compositions of mineralizing fluids at different types of porphyry deposits.

## 2. Overview of Deposits Discussed in This Publication

To analyze information on fluid inclusions in minerals from porphyry deposits, we have used the database compiled by V.B. Naumov at Vernadsky Institute of Geochemistry and Analytical Chemistry (GEOKhI), Russian Academy of Sciences [48]. This database comprises data from more than 22,700 publications devoted to melt and fluid inclusions and contains more than 116,500 determinations of the temperatures of mineralizing fluids and melts, 16,000 determinations of pressure, more than 67,500 determinations of fluid salinity, more than 130,000 analyses of concentrations of various elements in natural fluids, and information on fluid inclusions in minerals from more than 4200 deposits around the globe, e.g., [47–49]. We have searched the database for parameters of mineralizing fluids at approximately 60 porphyry deposits of various types in the Cu–Mo–Au system. All deposits discussed below (Table 1) can be technically classified with porphyry deposits. They belong to one of the four geochemical types (Cu (Au); Cu, Mo (Au); Mo; and Au), and their age ranges from the Paleozoic to Cenozoic (the ages are reported below, according to published data on the deposits). If the isotope age of any deposit was published, this age value is reported in Table 1; otherwise, the age is specified only as the geological period when this deposit was reportedly formed. We have not found any reliable published data on porphyry deposits whose age is older than Paleozoic, which is consistent with the viewpoint that erosion has destroyed most ancient porphyry deposits [50].

**Table 1.** Characteristics of porphyry deposits of different geochemical type.

Deposit, Country	Type *	Age, Ma	References
Bingham Canyon, USA	2	37.7–38.6	[51]
Butte, USA	2	66	[51]
Climax, USA	3	29.8	[51]
Copper Canyon, USA	1	Eocene? **	[52]
Kalmakyr, Uzbekistan	2	Paleozoic	[53]
Bingham Canyon, USA	2	37.7–38.6	[54]
Coloula, Papua New Guinea	1	1.5	[55]
Inguaran district, Mexico	1	50	[56]
Panguna, Papua New Guinea	1	Miocene	[57]
Red Mountain, USA	1	60	[58]
Sierrita, USA	1	57–59	[59]
Washington, Mexico	2	46	[60]
Mines Gaspé, Canada	2	Devonian	[61]
Santa Rita, New Mexico, USA	2	Paleocene	[62]
Cumobabi, Mexico	2	55.6–63.1	[63]
Wallapai mining district, USA	2	73	[64]
Bingham Canyon, USA	2	37.7–38.6	[65]
Park Premier Stock, USA	1	31–35	[66]
Questa, USA	3	24.2	[25]
Sungun, Iran	2	Miocene	[67]
Far Southeast, Philippines	4	1.3–1.4	[68]
Bajo de la Alumbrera, Argentina	1	6.1–9.7	[69]
Grasberg, Indonesia	1	2.6–4.4	[69]
Shotgun, USA	2	67	[70]
Bingham Canyon, USA	2	37.7–38.6	[71]
Bajo de la Alumbrera, Argentina	1	6.1–9.7	[72]
Santa Rita, New Mexico, USA	2	Paleocene	[73]
Bajo de la Alumbrera, Argentina	1	6.1–9.7	[74]
Escondida, Chile	1	34–36	[75]
Bajo de la Alumbrera, Argentina	1	6.1–9.7	[76]
Butte, USA	2	66	[29]

Table 1. Cont.

Deposit, Country	Type *	Age, Ma	References
Bingham Canyon, USA	2	37.7–38.6	[77]
Río Blanco, Chile	2	4.0–5.2	[78]
Rosario, Chile	2	32.6–34.5	[79]
Cerro Colorado, Chile	2	51.8	[80]
El Teniente, Chile	2	4.4–6.3	[81]
Bugdainskoe, Russia	2	Jurassic	[82]
Fenghuangshan, China	1	Jurassic–Cretaceous	[83]
Talatui, Russia	4	Jurassic	[84]
Butte, USA	2	66	[85]
Cave Peak, USA	2	32–39	[30]
La Caridad Antigua, Mexico	1	55	[86]
Questa, USA	3	24.2	[87]
Nevados de Famatina, Argentina	2	5.3	[88]
Xiongcu, China	1	14–39	[89]
Qiyugou, China	4	105–183	[90]
Bingham Canyon, USA	2	37.7–38.6	[91]
Bajo de la Alumbrera, Argentina	1	6.1–9.7	[91]
Bingham Canyon, USA	2	37.7–38.6	[92]
Baogutu, China	2	309–326	[93]
Qiyugou, China	2	105–183	[94]
Xishizishan, China	1	Triassic	[95]
Huashupo, China	1	Triassic	[95]
Datuanshan, China	1	Triassic	[95]
Tongguanshan, China	1	Triassic	[95]
Shizishan, China	1	Triassic	[95]
Shizishan, China	1	Triassic	[96]
Shaxi, China	1	128	[96]
Tongniujing, China	1	128	[96]
Xiaomiaoshan, China	1	128	[96]
Baocun, China	1	135–145	[97]
Datuanshan, China	1	135–145	[97]
Dongguashan, China	1	135–145	[97]
Chaoshan, China	1	135–145	[97]
Duobuza, China	1	121.6	[98]
Mount Leyshon, Australia	4	290	[99]
Dinkidi, Philippines	1	25.12	[100]
Bingham Canyon, USA	2	37.7–38.6	[101]
Novogodnee Manto, Russia	1	400	[102]
Biely Vrch, Slovakia	2	Miocene	[103]
Jinchang, China	1	110–120	[104]
Maher-Abad, Iran	1	Eocene	[105]
Peschanka, Russia	1	Cretaceous	[106]
Kighal, Iran	2	Eocene	[107]
Climax, USA	3	29.8	[108]
Malysh, Russia	3	Cretaceous	[109]
Peschanka, Russia	1	Cretaceous	[109]
Nakhodka, Russia	1	Cretaceous	[109]
Dexing, China	2	154–173	[110]
Vasil'kovskoe, Kazakhstan	4	279–312	[111]
Malmyzh, Russia	1	Cretaceous	[112]
Pebble, USA	2	90	[113]
Qarachilar, Iran	2	42.35	[114]
Machangqing, China	2	35.0	[115]
Yulong, China	2	43.2	[115]
Tongchang, China	2	34.0–35.8	[115]
Seleteguole, China	2	302–307	[116]
Malmyzh, Russia	1	96–128	[117]

Table 1. Cont.

Deposit, Country	Type *	Age, Ma	References
Grasberg, Indonesia	1	2.6–4.4	[118]
Nº 1, China	1	161.5	[119]
Kışladağ, Turkey	4	17.29–12.15	[120]
Grasberg, Indonesia	1	2.6–4.4	[121]
Sadaigoumen, China	3	240–243.7	[122]

Note. \* Types of porphyry deposits: 1–Cu (Au); 2–Cu, Mo (Au); 3–Mo; 4–Au. \*\* Presumably.

It is worth briefly considering the information contained in the database. Parameters of fluids are specified for individual samples, if this information is available from the literature. Hence, each data point in the diagram is based on the data on a great number of fluid inclusions. For a single individual sample, the database includes both the minimum and the maximum temperature values. In an analogous situation with salt concentrations otherwise, both the minimum and maximum salinity values are reported. These values were then used in the diagrams. Table 2 reports the minimum and maximum values of physicochemical parameters, for the ore mineralization of each deposit.

Table 2. Parameters of mineralizing fluids at porphyry deposits.

Deposit, Country, or Area	Physical Parameters of Fluid				Type ** of Deposit	References
	T, °C	S *, wt %	d, g/cm <sup>3</sup>	P, bar		
Bingham Canyon, USA	405 (1)	49.0	1.25	-	2	[51]
Butte, USA	275–335 (2)	1.0	0.62–0.76	-	2	[51]
Climax, USA	566 (1)	69.0	1.45	-	3	[51]
Copper Canyon, USA	250–345 (3)	1.2–40.0	0.80–1.06	-	1	[52]
Kalmakyr, Uzbekistan	375–800 (7)	33.8–69.0	0.94–1.20	1000–1500 (4)	2	[53]
Bingham Canyon, USA	350–616 (17)	42.0–53.0	0.95–1.21	-	2	[54]
Coloula, Papua New Guinea	400–700 (4)	34.0–62.0	0.60–1.30	1200 (1)	1	[55]
Inguaran district, Mexico	226–360 (17)	11.9–36.0	0.78–1.07	-	1	[56]
Red Mountain, USA	448–576 (6)	52.0–68.0	1.12–1.50	-	1	[58]
Washington, Mexico	364–550 (2)	34.5	0.81–0.98	-	2	[60]
Mines Gaspé, Canada	138–506 (68)	9.5–56.0	0.60–1.25	-	1	[61]
Santa Rita, USA	775 (1)	70.0	1.50	-	2	[62]
Cumobabi, Mexico	235–480 (8)	2.9–50.0	0.63–1.12	-	2	[63]
Questa, USA	150–500 (16)	2.0–57.0	-	800–1400 (8)	3	[25]
Sungun, Iran	215–605 (54)	2.2–59.8	0.54–1.12	-	1	[67]
Far Southeast, Philippines	450–550 (2)	48.5–55.0	1.07–1.25	-	4	[68]
Shotgun, USA	270–509 (8)	28.0–69.0	0.76–1.50	-	2	[70]
Bajo de la Alumbreira, Argentina	745–845 (2)	62.0	-	-	1	[74]
Escondida, Chile	270–680 (10)	3.0–67.0	0.68–1.23	-	1	[75]
Bajo de la Alumbreira, Argentina	615–845 (3)	45.0–53.0	-	-	1	[76]
Rosario, Chile	237–593 (31)	0.7–73.0	0.58–1.65	-	2	[79]
Cerro Colorado, Chile	90–544 (32)	0.1–52.0	0.60–1.30	-	2	[80]
El Teniente Deposit, Chile	262–515 (49)	2.1–60.5	0.47–1.15	-	2	[81]
Bugdainskoe, Russia	205–576 (11)	6.9–70.5	0.66–1.45	-	2	[82]
Fenghuangshan, China	122–620 (100)	3.4–71.5	0.63–1.40	-	1	[83]
Talatui, Russia	133–611 (50)	0.4–56.3	0.47–1.21	108–3366 (37)	4	[84]
Butte, USA	140–413 (14)	1.0–48.0	0.41–1.14	-	2	[85]
Questa, USA	271–429 (21)	2/8–50/0	0/43–1/12	-	3	[87]
La Caridad Antigua, Mexico	330–470 (13)	28.0–56.0	0.95–1.15	-	1	[86]

Table 2. Cont.

Deposit, Country, or Area	Physical Parameters of Fluid				Type ** of Deposit	References
	T, °C	S *, wt %	d, g/cm <sup>3</sup>	P, bar		
Nevados de Famatina, Argentina	175–552 (22)	1.5–64.4	0.46–1.48	-	2	[88]
Xiongcun, China	121–382 (37)	1.9–34.6	0.59–1.16	-	1	[89]
Qiyugou, China	157–460 (24)	3.7–37.2	0.58–1.02	-	4	[90]
Bingham Canyon, USA	323–492 (3)	34.7–50.4	0.90–1.10	-	2	[91]
Baogutu, China	151–550 (90)	0.2–66.8	0.46–1.22	307–3128 (9)	2	[93]
Qiyugou, China	109–476 (21)	3.9–47.0	0.65–1.10	-	4	[94]
Xishizishan, China	131–570 (7)	1.1–54.5	0.87–1.12	-	1	[95]
Huashupo, China	191–525 (10)	9.6–49.9	0.70–1.01	-	1	[95]
Datuanshan, China	205–437 (7)	7.6–43.8	0.72–1.09	-	1	[95]
Tongguanshan, China	289–885 (12)	6.0–44.9	0.64–1.16	-	1	[95]
Shizishan, China	148–600 (11)	2.1–56.2	0.52–1.10	-	1	[95]
Shizishan, China	158–610 (13)	2.1–56.2	0.56–1.19	-	1	[96]
Shaxi, China	110–520 (10)	8.0–58.0	0.71–1.13	-	1	[96]
Tongniujing, China	192–450 (3)	30.0–48.0	1.00–1.11	-	1	[96]
Xiaomiaoshan, China	91–369 (4)	0.7–43.0	0.81–1.14	-	1	[96]
Baocun, China	240–310 (4)	16.1–26.0	0.91–1.01	-	1	[97]
Datuanshan, China	160–440 (12)	8.7–29.3	0.67–1.03	-	1	[97]
Dongguashan, China	170–450 (7)	17.0–53.3	0.93–1.12	-	1	[97]
Chaoshan, China	220–280 (2)	17.0	0.91–0.98	-	1	[97]
Duobuza, China	616–957 (33)	34.0–74.0	0.75–1.80	400–1600 (15)	1	[98]
Mount Leyshon, Australia	150–595 (64)	0.2–61.9	0.38–1.13	-	4	[99]
Bingham Canyon, USA	313–610 (121)	3.3–59.0	0.42–1.21	-	2	[101]
Novoe Manto, Russia	100–365 (9)	9.6–24.2	0.86–1.15	-	1	[102]
Jinchang, China	200–620 (42)	0.4–74.0	0.40–1.55	-	1	[104]
Maher-Abad, Iran	150–488 (20)	9.5–47.9	0.80–1.13	-	1	[105]
Peschanka, Russia	205–506 (10)	0.2–55.0	0.4–1.11	-	1	[106]
Kighal, Iran	180–600 (6)	23.0–70.0	0.79–1.50	-	2	[107]
Malysz, Russia	129–545 (26)	0.7–47.0	0.55–1.09	270–470 (2)	3	[109]
Peschanka, Russia	104–506 (40)	0.2–55.7	0.43–1.36	220–540 (8)	1	[109]
Nakhodka, Russia	122–581 (10)	2.1–57.8	0.51–1.14	280–850 (3)	1	[109]
Dexing, China	105–524 (33)	1.1–63.0	0.58–1.19	1500–3000 (2)	2	[110]
Vasil'kovskoe, Kazakhstan	100–550 (126)	2.0–22.5	0.47–1.03	150–2300 (69)	4	[111]
Malmyzh, Russia	331–850 (9)	27.0–80.0	0.95–1.13	-	1	[112]
Pebble, USA	147–535 (157)	0.1–61.0	0.41–1.20	-	2	[113]
Qarachilar, Iran	190–530 (15)	9.2–55.0	0.65–1.12	-	2	[114]
Machangqing, China	202–550 (15)	12.7–22.1	0.51–1.09	-	2	[115]
Yulong, China	220–600 (20)	2.0–46.0	0.48–1.07	-	2	[115]
Tongchang, China	240–460 (15)	2.0–52.0	0.80–1.13	-	2	[115]
Seleteguole, China	268–483 (54)	2.1–57.4	0.48–1.14	-	2	[116]
Malmyzh, Russia	260–525 (10)	0.4–60.0	0.45–1.14	500 (2)	1	[117]
Grasberg, Indonesia	255–700 (25)	6.4–74.7	0.48–1.12	-	1	[118]
№ 1, China	132–522 (104)	0.9–62.8	0.41–1.19	-	1	[119]
Kışladağ, Turkey	250–600 (35)	1.0–49.0	0.47–1.04	-	4	[120]
Grasberg, Indonesia	228–700 (403)	1.4–88.0	0.625–1.47	-	1	[121]
Sadaigoumen, China	211–510 (122)	1.2–50.6	-	10–600 (8)	3	[122]

Note: \* fluid salinity in wt % equiv. NaCl (numerals in parentheses show the number of determinations); \*\* types of porphyry deposits: 1–Cu (Au); 2–Cu, Mo (Au); 3–Mo; 4–Au.

Some publications dealing with multiphase fluid inclusions of high-temperature chloride brines report salinity values calculated as the total concentrations of NaCl (calculated from the dissolution temperatures of halite) and KCl (calculated from the dissolution temperatures of sylvite), which are collectively reported as equivalent NaCl concentrations.

Due to this, some data points in the salinity–temperature diagrams plot to the right of the concentration line of saturated NaCl solution at various temperatures, but these points occur to the left of the saturated KCl solution line.

Assemblages of fluid inclusions are very rarely distinguished in minerals at porphyry deposits, since it is very difficult to prove that different types of the fluid inclusions (used to calculate the pressures) were indeed captured simultaneously. Due to this, data on the pressures of mineralizing fluids at porphyry deposits are still insufficient and are not discussed herein.

Some values of aqueous fluid density at some porphyry deposits were not quoted in the source publications, but we calculated them from data on the temperature and salinity of the fluid using FLINCOR (1.x) software, USA [123].

The deposits discussed in this paper are located in all major regions of porphyry deposits worldwide (Figure 1): the eastern shore of North and South America (USA, Canada, Argentina, and Chile), various parts of Eurasia, including eastern Europe, southern, middle, and central Asia (Slovakia, Russia, Kazakhstan, Iran, Turkey, and China), and Pacific islands (Philippines, Papua New Guinea, and Indonesia).



**Figure 1.** Location map of the porphyry deposits discussed in this publication. Types of porphyry deposits: 1—Cu (Au); 2—Cu, Mo (Au); 3—Mo; 4—Au. Deposits: 1—Bugdainskoe, Russia; 2—Malysh, Russia; 3—Peschanka, Russia; 4—Novogodnee Manto, Russia; 5—Malmyzh, Russia; 6—Nakhodka, Russia; 7—Kalmakyr, Uzbekistan; 8—Wallapai mining district, USA; 9—Sierrita, USA; 10—Shotgun, USA; 11—Red Mountain, USA; 12—Pebble, USA; 13—Park Premier Stock, USA; 14—Copper Canyon, USA; 15—Climax, USA; 16—Cave Peak, USA; 17—Butte, USA; 18—Bingham Canyon, USA; 19—Kışladağ, Turkey; 20—Biely Vrch, Slovakia; 21—far southeast, Philippines; 22—Panguna, Papua New Guinea; 23—Koloula, Papua New Guinea; 24—Washington, Mexico; 25—La Caridad Antigua, Mexico; 26—Inguaran district, Mexico; 27—Cumobabi, Mexico; 28—Vasil’kovskoe, Kazakhstan; 29—Sungun, Iran; 30—Qarachilar, Iran; 31—Maher-Abad, Iran; 32—Kighal, Iran; 33—Grasberg, Indonesia; 34—Yulong, China; 35—Xionggun, China; 36—Xiaomiaoshan, China; 37—Tongniujiang, China; 38—Tongchang, China; 39—Shizishan, China; 40—Shaxi, China; 41—Seleteguole, China; 42—Qiyugou, China; 43—No. 1, China; 44—Machangqing, China; 45—Jinchang, China; 46—Fenghuangshan, China; 47—Duobuza, China; 48—Dexing, China; 49—Baogutu, China; 50—Baocun, China; 51—Rosario, Chile; 52—Río Blanco, Chile; 53—Escondida, Chile; 54—El Teniente, Chile; 55—Cerro Colorado, Chile; 56—Mines Gaspé, Canada; 57—Granisle, Canada; 58—Dublin Gulch, Canada; 59—Bell, Canada; 60—Mount Leyshon, Australia; 61—Nevados de Famatina, Argentina; 62—Bajo de la Alumbra, Argentina; 63—Santa Rita, USA.

Note that our selection includes such widely known porphyry deposits of various types as Peschanka (type 1) and Malmyzh (type 1) in Russia; Kalmakyr (type 2) in Uzbekistan; Pebble (type 2), Climax (type 3), Butte (type 2), and Bingham Canyon (type 2) in

the USA; Kışladağ (type 4) in Turkey; Grasberg (type 1) in Indonesia; and others. This provided us with enough solid ground, to hope that the data analyzed in this publication are representative enough for solving the formulated problems.

### 3. Characterization of Fluids at Porphyry Deposits

When fluid inclusions are characterized, their descriptions are, conventionally, begun with descriptions of how these inclusions look like at room temperature. Fluid inclusions hosted in minerals from porphyry deposits can be grouped into the following three types, according to the phase composition of these inclusions at room temperature (Figure 2).

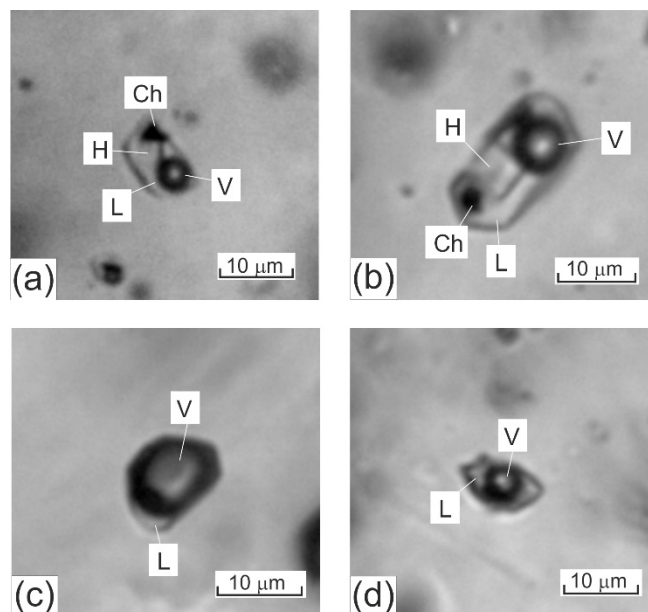


**Figure 2.** Three major types of fluid inclusions typically hosted in quartz from mineralized veinlets at porphyry deposits: (a,b) fluid inclusions of high-temperature chloride brines (the photos show dark gas bubbles, transparent cubic NaCl crystals, opaque chalcopyrite crystals, and solution); (c) gas fluid inclusions (the photos show a gas phase and a pale rim of aqueous solution); (d) two-phase gas–liquid inclusions of aqueous solutions of intermediate salinity (the photos show a roundish gas phase and pale aqueous salt solution). The scale bars are 10 µm. L–aqueous solution, V–gas phase, H–halite, Ch–chalcopyrite.

**Type 1.** Fluid inclusions of high-salinity brines: these inclusions contain an aqueous solution of high salinity (>26–30 wt % equiv. NaCl), a vapor bubble, and one or more daughter crystals. Among the latter, halite, sylvite, opaque or transparent red crystals of hematite and anhydrite have been identified [34]. The triangular transparent phases are usually identified as chalcopyrite crystals [26,31,34], which provide evidence of a high Cu concentration in the fluid. Recent Raman spectroscopic studies have identified daughter phases of javorieite  $KFeCl_3$  [124] and magnetite [125].

**Type 2.** Gas-rich fluid inclusions ( $> 70 \pm 10$  vol % gas).

**Type 3.** Aqueous salt two-phase fluid inclusions, whose salinity ranges from low to intermediate, and which contain a gas bubble that occupies  $30 \pm 10$  vol %.

Some authors, [46] and others, distinguish an individual type of gas fluid inclusions of intermediate density, which contains an aqueous solution and vapor in equal proportions ( $L \approx V$ ), and which, also, sometimes host a small opaque crystal. It is thought that these fluid inclusions captured magmatic fluid at a high temperature and pressure in the region of homogeneous fluid above the vapor–liquid boundary in the system  $H_2O$ –NaCl, and sometimes contain  $CO_2$  [51,85,87]. Such fluid could be entrapped in fluid inclusions at deeper levels than those where the ore mineralization was deposited. Due to this, such

fluid inclusions cannot be numerous, and they cannot significantly modify the general situation. Herein, we attribute these inclusions to type 2, if such inclusions are mentioned in publications.

Figure 3 and Table 2 show the variations of parameters of mineralizing fluids collectively for all of the fluid inclusions, without subdividing them into types, but only the general ranges of the homogenization temperatures, salinity, and densities of the fluids. Note that the data on low-density fluid inclusions containing a gas phase can be incomplete due to purely technical reasons, namely, due to the small volumes of aqueous fluids in these inclusions, which often make it impossible to microthermometrically study these inclusions. This shall be taken into account when dealing with the data on fluid inclusions. The gas constituent of mineralizing fluid at porphyry deposits is not discussed in this paper because such information is still insufficient and because this information cannot characterize all types of porphyry deposits.

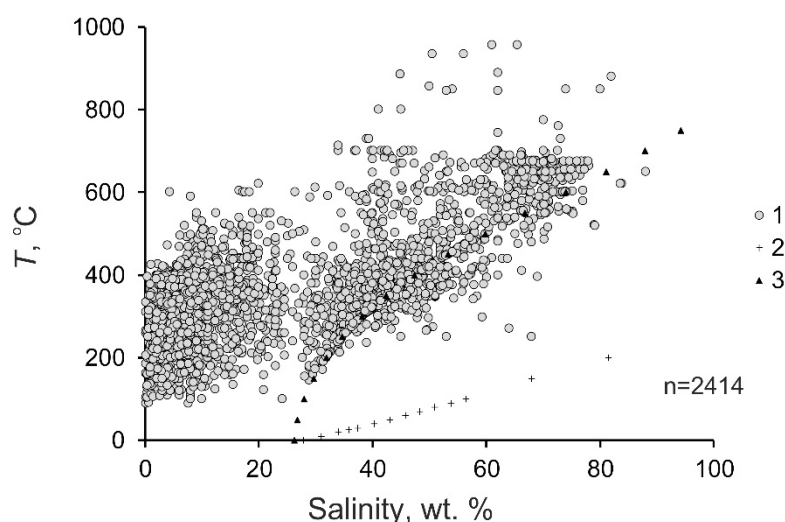


**Figure 3.** Diagram temperature–salinity for mineralizing fluids at porphyry deposits. 1—fluids at the deposits; 2—saturated KCl solution; 3—saturated NaCl solution.

Overall ranges of the physicochemical parameters. The principal parameters of mineralizing fluids at individual porphyry deposits of various types in the Cu–Mo–Au system are listed in Table 2. In general, the ranges of the principal physicochemical parameters of fluids at porphyry deposits are fairly broad, as follows from the data on 2414 groups of fluid inclusions (Figure 3, Table 3): the homogenization temperatures of the fluid inclusions range from 90 to 957 °C (388 °C on average). As seen in the histogram in Figure 4, most of the fluids were entrapped into fluid inclusions at temperatures of 200 to 500 °C. Note that publications usually present homogenization temperatures of fluid inclusions. However, it is now acknowledged that mineral-forming processes at porphyry deposits begin when the fluid becomes heterogeneous [32,33]. It is known that if fluid inclusions are entrapped on a two-phase equilibrium curve, the homogenization temperatures of these inclusions are equal to their entrapment temperatures [34]. Hence, the homogenization temperatures of early mineral-hosted fluid inclusions at porphyry deposits usually correspond to their entrapment temperatures, which allowed us to discuss the fluid temperatures here.

It shall be mentioned that some papers report homogenization temperatures of fluid inclusions higher than 600 °C, with these values obtained using high-temperature heating stages. Such data usually provoke no doubts, if the publication reports information that these data are reproducible. However, we rejected homogenization temperatures above 700 °C (up to 1290 °C) obtained for the Grasberg deposit [118,121], since the authors themselves were not sure whether these values do characterize the processes that produced the ores. Indeed, fluids at porphyry deposits contain much Fe and can lose protons because of water dissociation when heated to very high temperatures; the protons can migrate from

the fluid inclusions through their host quartz and, thus, irreversibly change the composition of the fluid inclusions and result in overestimates of their homogenization temperatures, e.g., [34,126,127].

**Table 3.** Parameters of mineralizing fluids at porphyry deposits of different types.

Types * of Deposits	n	Temperature, °C			Salinity, wt. %			Density of Fluid, g/cm <sup>3</sup>		
		Interval	Average Arithmetic	Average Geometric	Interval	Average Arithmetic	Average Geometric	Interval	Average Arithmetic	Average Geometric
All	2414	90–957	388	372	0.1–88.0	29.4	28.2	0.38–1.85	0.93	0.95
1	1017	91–957	437	421	0.2–88.0	39.4	41.4	0.40–1.85	1.00	1.00
2	923	90–800	359	363	0.1–73.0	26.3	28.6	0.41–1.65	0.91	0.96
3	193	129–566	349	354	0.7–69.0	13.8	8.5	0.43–1.45	0.85	0.83
4	280	100–611	329	341	0.2–61.9	13.0	9.0	0.38–1.25	0.81	0.81

Note: \* types of porphyry deposits: 1–Cu (Au); 2–Cu, Mo (Au); 3–Mo; 4–Au; n: number of measurements.

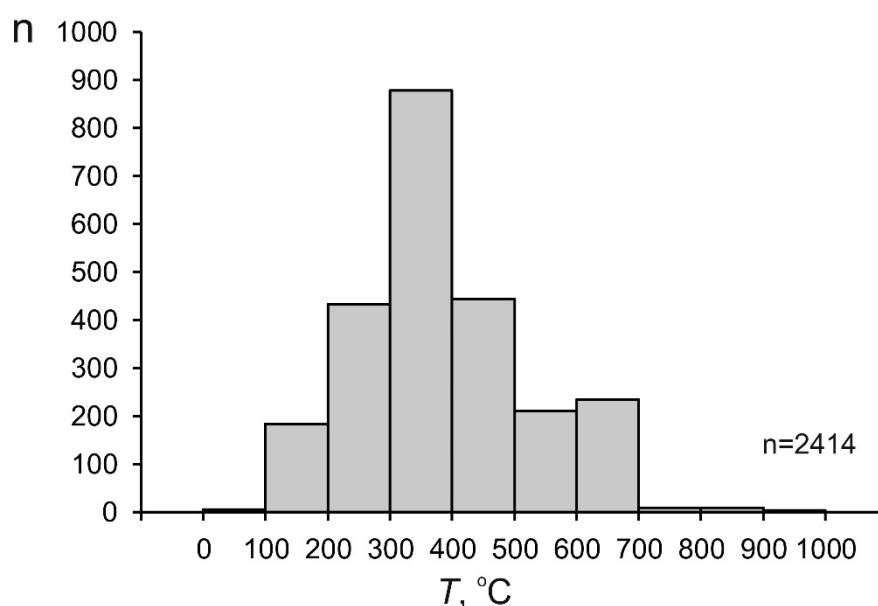


**Figure 4.** Histogram of the temperature of mineralizing fluids at porphyry deposits.

The salinity of the mineralizing fluids varies from 0.1 to 88.0 wt % equiv. NaCl (29.4 wt % equiv. NaCl on average). Some salinity values of fluids at porphyry deposits extend outside the H<sub>2</sub>O–NaCl saturation line, but they are no higher than the KCl solubility. (Figure 3). This is consistent with the sylvite that was found among the daughter minerals in fluid inclusions and with the occurrence of potassic metasomatites at porphyry deposits. The histogram of the salinity of the fluids has two maxima, at 0 to 10 and 35 to 45 wt % (Figure 5). This reflects the heterogenization of fluid, a process during which porphyry deposits start to be formed.

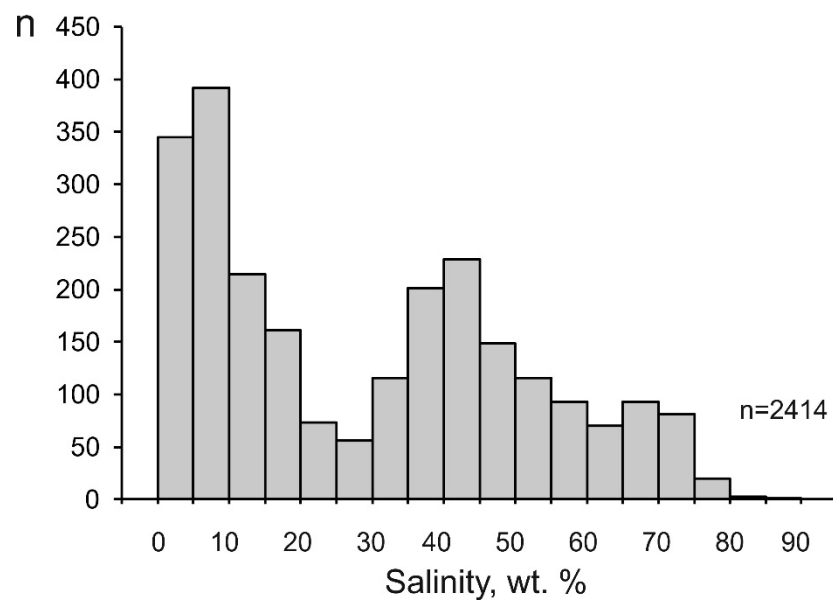


**Figure 5.** Histogram of the salinity of mineralizing fluids at porphyry deposits.

The density of mineralizing fluids at porphyry deposits also varies broadly, from 0.33 to 1.85 g/cm<sup>3</sup> (average 0.93 g/cm<sup>3</sup>), since this parameter is interrelated with, first of all, the temperature and salinity of the fluids. The maximum variations in the fluid density were found at temperatures above 300 °C (Figure 6), which is also related to the heterogenization of the fluids. Below 200 °C, the density of the fluids approaches 1 g/cm<sup>3</sup> because of the temperature decrease and the occurrence of the fluid in the homogeneous region. The histogram of the fluid density is unimodal, with its maximum occurring at 1.00 to 1.10 g/cm<sup>3</sup> (Figure 7).

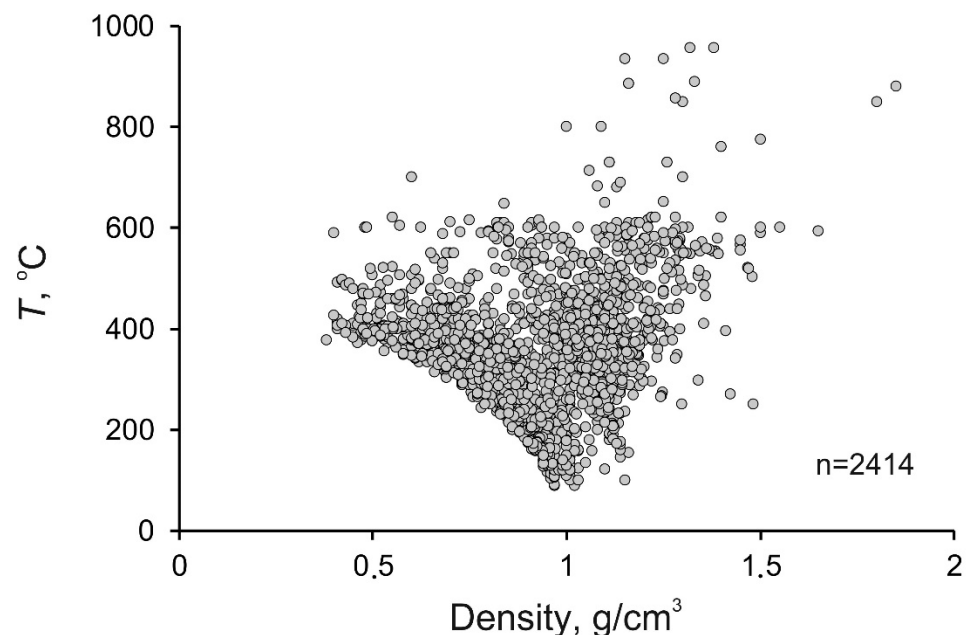


**Figure 6.** Diagram temperature–density for mineralizing fluids at porphyry deposits.

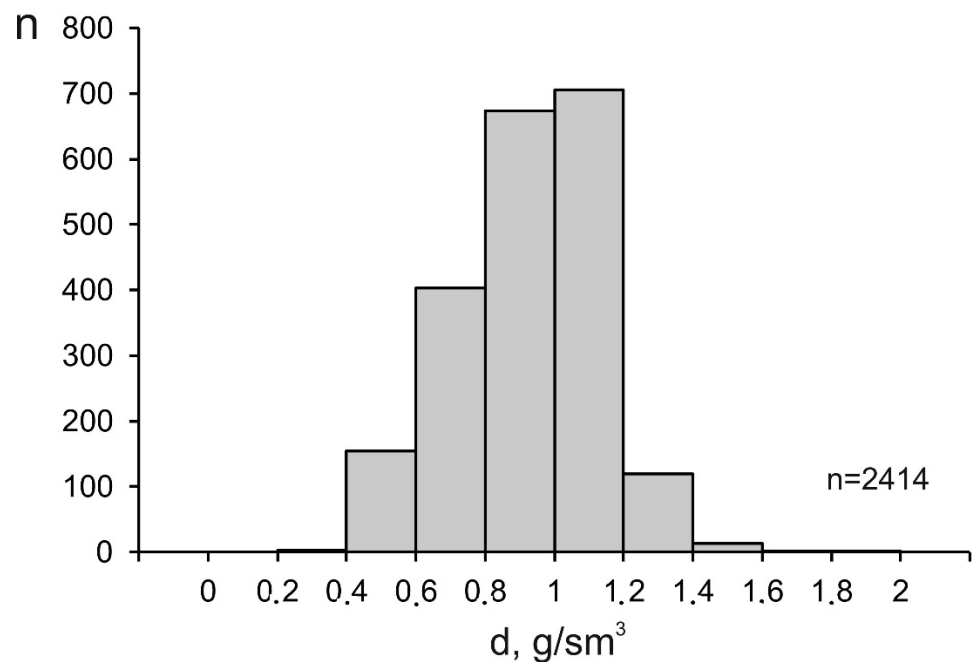


**Figure 7.** Histogram of the density of mineralizing fluids at porphyry deposits.

Some systematic differences were found between the average and maximum values of the parameters of the mineralizing fluids at porphyry deposits of various types (Table 3, Figure 8).

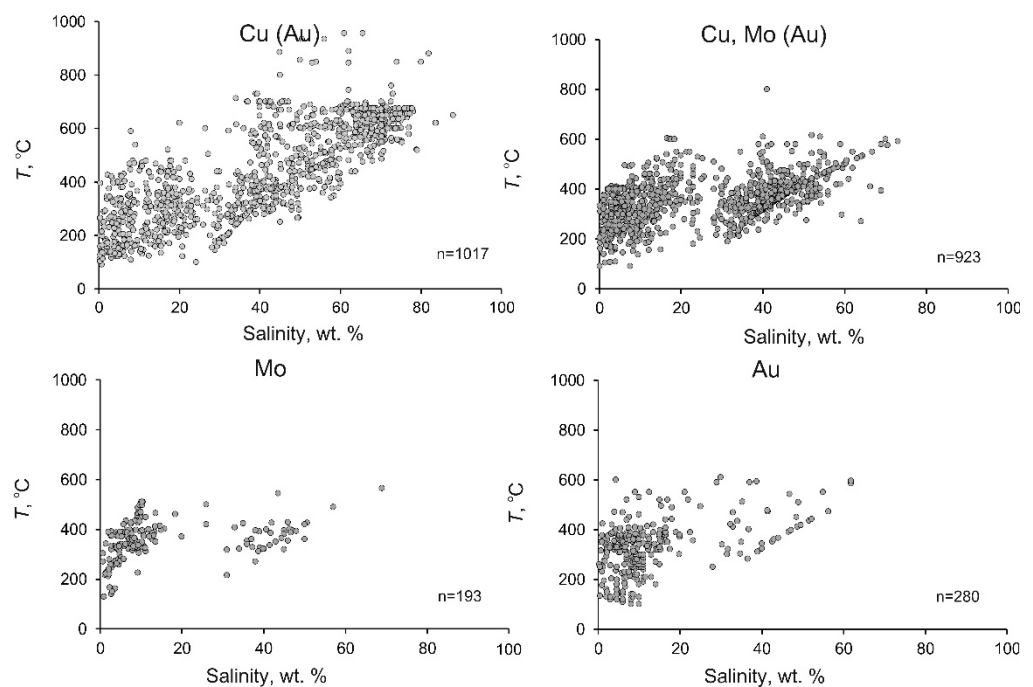


**Figure 8.** Temperature–salinity diagram for mineralizing fluids at porphyry deposits of different types.

The average homogenization temperatures, salinity, and density of the fluids at deposits of various types commonly systematically decrease from deposits of type 1 to those of type 4. Figure 8 shows that the variations of the homogenization temperatures and salinity of the fluids at deposits of various types are generally similar, but the fields of these variations systematically shrink. This situation is not universal for the maximum homogenization temperatures. The minimum values of the maximum homogenization tem-

peratures of fluids were found at porphyry Mo deposits (type 3), which may be explained by the fact that the numbers of measurements at deposits of types 3 and 4 are smaller.

The great scatter of fluid parameters at each deposit (for example, the temperature ranges within a few hundred grades) inevitably puts forth the problem of the significance of the detected differences (for example, the average temperatures vary within as little as 10–40 °C) between the average parameters of fluids at porphyry deposits of different types. To sort out anomalous outlier values and be able to more accurately compare available data on various parameters, including those in the regions with 50% of the data (Figure 9), we have constructed boxplots. The diagram for the temperatures (Figure 9), obviously, shows that porphyry copper deposits of type 1 are noted for the highest maximum and average homogenization temperatures of fluid inclusions. Porphyry copper–molybdenum deposits of type 2 show intermediate values of the average and maximum temperatures, and porphyry molybdenum deposits of type 3 and porphyry gold deposits of type 4 are relatively low temperature. The situation with the salinity diagrams is generally analogous for the maximum and average values of this parameter (Figure 9). The highest salinity is typical of fluids at porphyry copper deposits of type 1, intermediate salinity values were found in fluids at porphyry molybdenum deposits of type 2, and the lowest values were detected in fluids at molybdenum deposits of type 3 and porphyry gold deposits of type 4. It should be mentioned that fluids at porphyry molybdenum deposits of type 3 and porphyry gold ones of type 4 yield the narrowest ranges of the dominant salinity values of the fluids. The density values of the fluids do not vary as widely (Figure 9), but the average density of the fluids, obviously and systematically, decreases from type 1 (Cu(Au)) to type 4 (Au). This led us to the conclusion that mineralizing fluids at porphyry deposits of different types are different in composition and have different parameters.

Here and in Figure 10, lines in the boxes are medians, crosses are averages, and spots are outliers (<https://towardsdatascience.com/understanding-boxplots-5e2df7bcbd51>, accessed on 11 September 2018).

Interesting information can be derived from analysis of data on concentrations of some elements in mineralizing fluids at porphyry deposits. The overall ranges of concentrations of dominant anions, cations, and ore elements in mineralizing fluids at porphyry deposits in the Cu–Mo–Au system are reported in Table 4. The concentrations of all elements (in ppm) are very broadly scattered: Cl 1200–941 000, S 200–66 300, Na 562–350 000, K 200–267 000, Ca 20–150 000, Mg 5.4–152 000, Cu 0.77–95 680, Fe 20–383 614, Zn 12–21 400, Mo 1.7–6400, W 1.0–3829, Sn 0.09–2200, 3–55 000, Au 0.07–107.8, and Ag 1.0–3370. This is fully consistent with the broad ranges of fluid salinity. Regrettably, no published data are available as of yet on S, Sn, and Au concentrations in fluids of type 4 (porphyry gold) deposits, which hampers analysis of gold behavior in the porphyry systems (Table 4). We have calculated the average and median concentrations of the aforementioned elements (Table 5) and constructed the boxplots (Figure 10). The distribution of the maximum concentrations of several elements (Cu, Fe, Zn, Pb, and others) generally is analogous to the distribution of the temperatures, i.e., the maximum concentrations of most elements are typical of fluids at deposits of type 1 (porphyry copper with gold). However, the Mo and Ag concentrations do not comply with this tendency. The maximum Mo concentrations, obviously, occur in fluids of deposits of type 3 (porphyry molybdenum deposits), whereas the highest Ag concentrations were found in fluids at type-4 (porphyry gold) deposits. The geochemical differences between fluids that produce porphyry deposits of different types pertain not only to the temperature, total salinity, and density of these fluids, but also to their concentrations of metals, which predetermine the metallogenic features of porphyry deposits of different types.

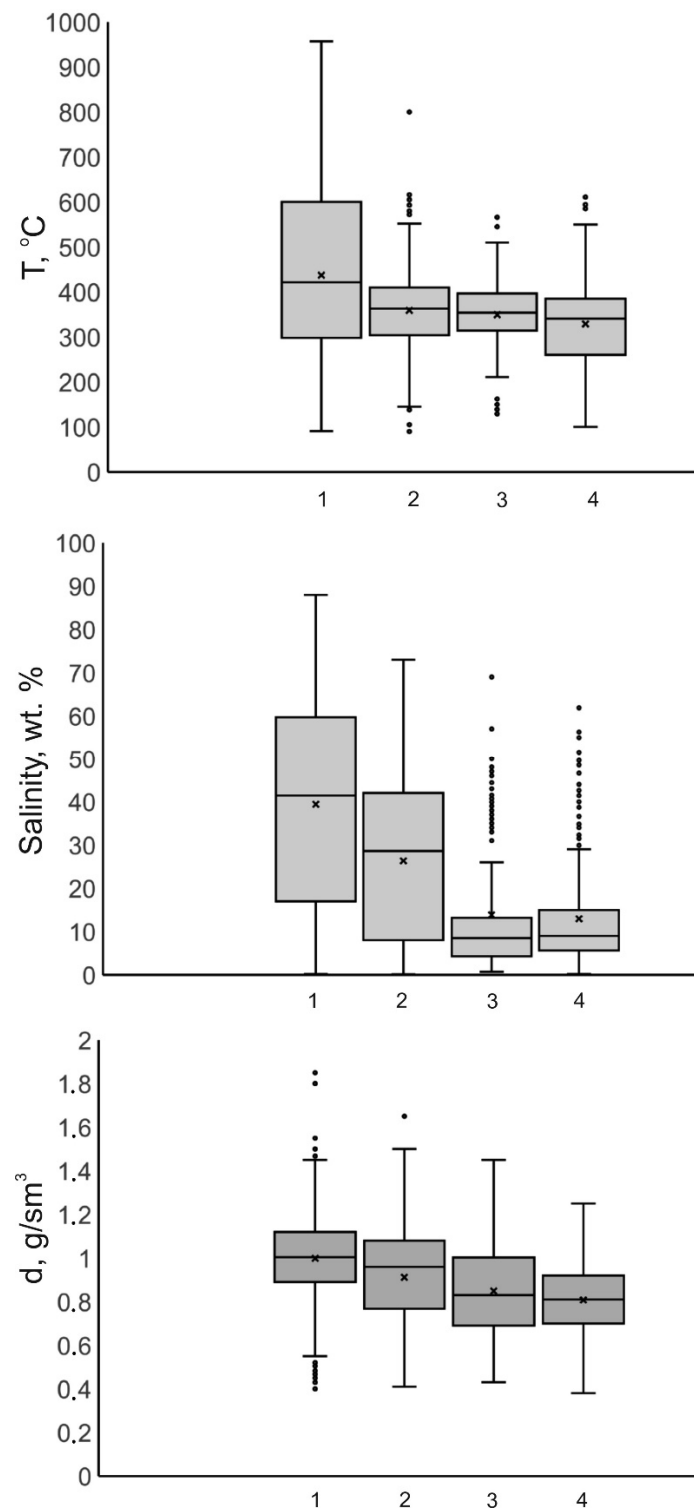


**Figure 9.** Boxplots for the homogenization temperatures of fluid inclusions, for the salinity of mineralizing fluids and for the density of mineralizing fluids at porphyry deposits of various types (1–Cu (Au); 2–Cu, Mo (Au); 3–Mo; 4–Au).

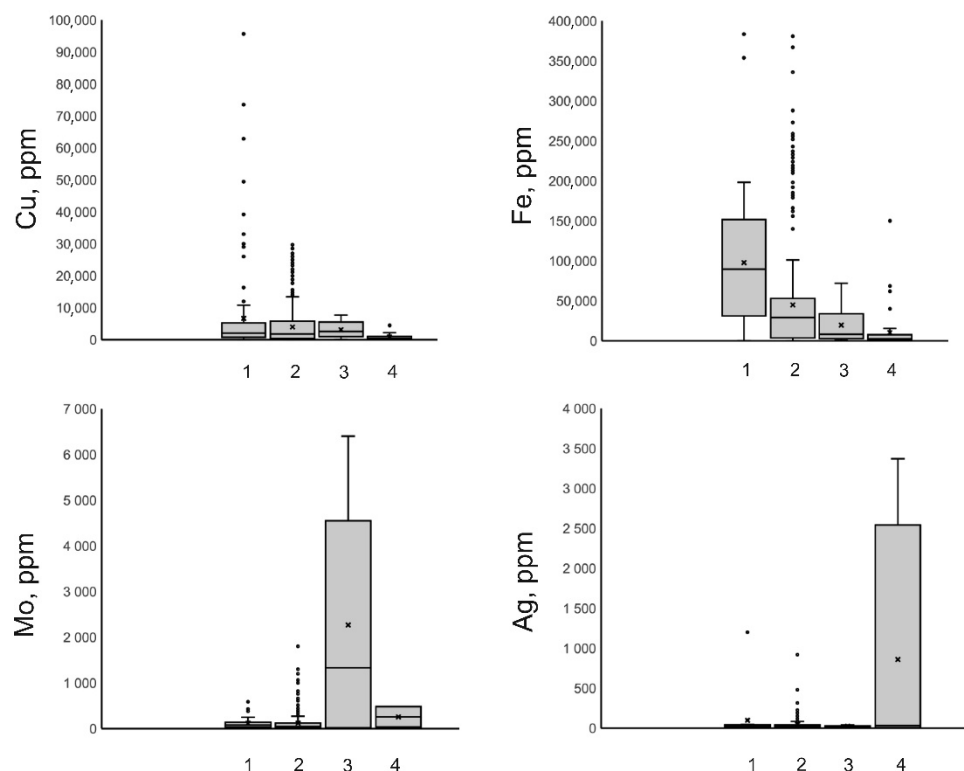


**Figure 10.** Boxplots for concentrations of Cu, Fe, Mo, and Ag, in mineralizing fluids at porphyry deposits of various types (1–Cu (Au); 2–Cu, Mo (Au); 3–Mo; 4–Au).

**Table 4.** Concentrations (ppm) of some elements in mineralizing fluids at porphyry deposits \*.

Element	Number of Determinations	Concentration (from–to)	Average		Types ** of Deposits
			Arithmetic	Geometric	
Cl	152	1200–941,000	218,849	74,010	1, 2, 3, 4
S	191	200–66,300	9488	6930	1, 2, 3
Na	760	562–350,000	63,957	37,400	1, 2, 3, 4
K	779	200–267,000	49,791	29,590	1, 2, 3, 4
Ca	254	20–150,000	13,214	7065	1, 2, 3, 4
Mg	220	5.4–152,000	5197	468	1, 2, 3, 4
Cu	696	0.77–95,680	4303	1900	1, 2, 3, 4
Fe	709	20–383,614	48,321	26,500	1, 2, 3, 4
Zn	538	12–21,400	2569	1700	1, 2, 3, 4
Mo	470	1.7–6400	219	50	1, 2, 3, 4
W	269	1.0–3829	172	26	1, 2, 3, 4
Sn	174	0.09–2200	266	25.6	1, 2, 3
Pb	600	3–55,000	1609	578	1, 2, 3, 4
Au	181	0.07–107.8	3.65	1.0	1, 2, 3
Ag	224	1.0–3370	62.7	19.5	1, 2, 3, 4

Note: \* data from [29,30,65,71–74,77,78,81,87,88,91,92,99–101,103,108,118]. \*\* Type of porphyry deposits: 1–Cu (Au); 2–Cu, Mo (Au); 3–Mo; 4–Au.

**Table 5.** Concentrations (ppm) of some elements in mineralizing fluids at porphyry deposits \* of various types.

Element	Number of Determinations	Concentration (from-to)	Average		Types ** of Deposits
			Arithmetic	Geometric	
Cl	9	<b>9500–464,000</b>	198,566	215,560	1 Cu (Au)
Cl	56	10412– <b>941,000</b>	440,686	<b>452,500</b>	2 Cu, Mo (Au)
Cl	11	190000–390,000	303,636	280,000	3 Mo
Cl	76	1200–375,000	<b>45,520</b>	31,000	4 Au
S	10	1618–36,648	<b>11,382</b>	5671	1 Cu (Au)
S	171	200– <b>66,300</b>	9633	<b>7100</b>	2 Cu, Mo (Au)
S	10	2640–7260	5115	5115	3 Mo
Cu	114	1– <b>95,680</b>	<b>6659</b>	2045.5	1 Cu (Au)
Cu	521	0.77–29,680	3983	1800	2 Cu, Mo (Au)
Cu	47	58–7700	3160	<b>2600</b>	3 Mo
Cu	14	51–4480	876	410	4 Au
Fe	103	195– <b>383,614</b>	<b>97,807</b>	<b>89,600</b>	1 Cu (Au)
Fe	507	101.4–381,000	44,866	29,000	2 Cu, Mo (Au)
Fe	45	630–72,000	19,663	8200	3 Mo
Fe	54	20–150,000	10,254	2400	4 Au
Mo	70	2–600	117	77.5	1 Cu (Au)
Mo	376	1.7–1800	118	42	2 Cu, Mo (Au)
Mo	22	1.78– <b>6400</b>	<b>2267</b>	<b>1330</b>	3 Mo
Mo	2	32–480	256	256	4 Au
W	17	1–160	47.9	22	1 Cu (Au)
W	228	2–1900	68.4	25	2 Cu, Mo (Au)
W	21	6– <b>3829</b>	<b>1420</b>	<b>183</b>	3 Mo
W	2	62–77	69.5	69.5	4 Au
Sn	9	0.09–1400	<b>529</b>	<b>570</b>	1 Cu (Au)
Sn	146	0.85– <b>2200</b>	264	150	2 Cu, Mo (Au)
Sn	19	15–398	160	76	3 Mo
Pb	109	40–15,000	<b>2621</b>	<b>2566</b>	1 Cu (Au)
Pb	454	3– <b>55,000</b>	1412	455	2 Cu, Mo (Au)
Pb	21	224–3532	1464	1099	3 Mo
Pb	16	21–2740	479	155	4 Au
Zn	49	49.4–18,300	<b>5317</b>	<b>4800</b>	1 Cu (Au)
Zn	391	12–16,000	2271	1700	2 Cu, Mo (Au)
Zn	47	57.6–15,000	3014	1214	3 Mo
Zn	51	46– <b>21,400</b>	1807	960	4 Au
Au	10	0.3–10.2	1.7	0.8	1 Cu (Au)
Au	168	0.07– <b>107.8</b>	<b>3.8</b>	<b>1.1</b>	2 Cu, Mo (Au)
Au	3	0.1–0.2	0.1	0.1	3 Mo
Ag	16	3–1200	98	20	1 Cu (Au)
Ag	193	1–919	45.5	19	2 Cu, Mo (Au)
Ag	11	11–38	22.9	22	3 Mo
Ag	4	2.2– <b>3370</b>	<b>858</b>	<b>30.8</b>	4 Au

Note: \* data from [29,30,65,71–74,77,78,81,87,88,91,92,99–101,103,108,118]. Numerals printed in bold are the maximum concentrations of a given element in each column. \*\* Type of porphyry deposits: 1–Cu (Au); 2–Cu, Mo (Au); 3–Mo; 4–Au.

#### 4. Discussion

The different minimum and maximum values of parameters of mineralizing fluids at porphyry deposits of different types in the Cu–Mo–Au system generally do not contradict either the results of earlier studies, e.g., [31,46,47], or the current understanding of processes that produce porphyry deposits, e.g., [8,33,40]. All parameters of mineralizing fluids (their temperature, salinity, and density) at porphyry deposits broadly vary, as do the concentrations of cations, anions, and metals, which confirms that porphyry deposits are formed where and when the mineralizing fluids become heterogeneous [33].

Some recently published papers present data that expand the temperature ranges of fluids at porphyry deposits. We rejected the highest values due to reasons discussed

above [118,121]. Among the rest of the data, the highest temperature is 957 °C [98], which is generally consistent with earlier estimates: >900 °C in [31] and 700 °C in the review [47].

The range of the fluid salinity values obtained from analyzing the literature data is also broad (0.1–88.0 wt % equiv. NaCl), but it is generally consistent with the parameters presented in [46], from 0 to 75 wt % equiv. NaCl, [31] from 0 to >60 wt % equiv. NaCl, and [47] from 0.1 to 70.0 wt % equiv. NaCl, which only slightly shifts the upper limit. Analogously, the range of the density values of the mineralizing fluids (0.38–1.85 g/cm<sup>3</sup>) generally does not contradict earlier estimates: from 0.01 to >1.00 g/cm<sup>3</sup> [46] and from 0.20 to 1.60 g/cm<sup>3</sup> [47].

Differences between the parameters of fluids at porphyry deposits of different types have still been discussed in the literature only with reference to porphyry copper and porphyry molybdenum systems, and this problem is still inadequately discussed in the literature. Information that fluids at porphyry copper deposits are generally higher temperature than fluids at porphyry molybdenum deposits can be found in [31,47]. This information is consistent with our data. However, we are the first to compare the parameters of mineralizing fluids at porphyry deposits of the four types in the Cu–Mo–Au system. The use of boxplots allowed us to demonstrate (Figure 9) that the highest fluid temperatures are typical of porphyry copper deposits (type 1), intermediate values occur at porphyry copper–molybdenum deposits (type 2), and the lowest temperatures are persistently determined in fluids at porphyry molybdenum (type 3) and porphyry gold (type 4) deposits. Other parameters of the mineralizing fluids (their salinity and density) vary analogously to the temperature variations, depending on the type of the deposit (Figure 10).

Data on concentrations of ore elements reported in this publication are generally consistent with preexisting information [31,46,47]. The greatest differences were caused by data in the most recent publications and do not modify the overall situation. However, we are the first to analyze the distributions of concentrations of ore elements in fluids at porphyry deposits of different types in the Cu–Mo–Au system. It is worth recalling that higher Mo concentrations, in mineralizing fluids at Mo deposits rather than in fluids in barren fluid–magmatic systems, were mentioned in [30], but these authors discussed a broad spectrum of various Mo deposits, including those of the porphyry type, and discussed general problems related to the origin of Mo-rich magmatic mineralizing fluid. In contrast to these authors, we focused on the behaviors of some ore elements in mineralizing fluid at porphyry deposits of various types.

It has been demonstrated above that the distribution of the Cu and Fe concentrations coincides with the distribution of the highest temperatures of the mineralizing fluids: the highest concentrations of these elements were found in mineralizing fluids at deposits of type 1, and these concentrations systematically decrease to deposits of type 4, as the temperatures do also. This is consistent with one of the conclusions in [46], that temperature is one of the principally important factors that controls concentrations of ore elements in fluids at porphyry deposits.

However, two elements behave differently from the others. The maximum Mo concentrations were found in fluids at porphyry Mo deposits, and the highest Ag concentrations were detected at porphyry Au deposits. This can hardly be incidental, and reasons for these differences in the Mo and Ag concentrations may not be related to temperature.

Different types of porphyry deposits in the Cu–Mo–Au system were, thus, formed by fluids whose physicochemical parameters and compositions were different. This raises the question as to when these differences, which result in porphyry-type mineralization of different types, were formed. When ore minerals are deposited after the fluid has become heterogeneous, processes may proceed that result in the spatial separation of various mineral associations, as has been demonstrated in [101], with reference to copper and molybdenum mineral associations. However, it is reasonable to anticipate that these phenomena and processes shall occur at the scale of a single deposit and predetermine its geochemical zoning, but do not modify its geochemical type.

Recall that, according to the current concept of the genesis of porphyry deposits, ore mineralization is deposited by magmatic fluids at shallow depths, within narrow pressure ranges, which allows the fluids to become heterogeneous. At the same time, magmatic fluid separates from the melt within a greater range of depths, from 5 to 10 km, e.g., [4]. The solidus temperature of granite melt, a parameter controlling the separation of magmatic fluid from crystallizing melt, decreases with depth because of an increase in the content of volatiles in melts. A change in parameters under which fluid is separated from melt can also be related to a change in the composition of the separating fluid. The detected change in the average fluid temperatures at various types of porphyry deposits is, perhaps, correlated with the temperature at which the magmatic fluid separated from the melt. If so, the same factor should have predetermined the geochemical features of the mineralizing fluids. A scenario, which can describe the separation of mineralizing fluids that produced different types of porphyry deposits from granite melt at various depths, is schematically represented in Figure 11. This schematic representation is based on the solidus of granite melt, from the widely known diagram [17]. According to Burnham's classic model, magmatic fluid separates from granite melt at its crystallization. The crystallization temperature of melts decreases with depth because of an increase in concentrations of volatiles in these melts. This correlates with the decrease in the mean and maximum fluid temperatures at porphyry deposits of various types in the sequence: Cu (Au); Cu, Mo (Au); Mo; and Au. We believe that the composition of fluids separating from melts varies with increasing pressure, according to the variations in the maximum fluid temperatures at various types of porphyry deposits, as schematically shown in Figure 11. However, fluids of various types start to deposit minerals at roughly the same depth level, when fluids ascend and, eventually, come to regions of low pressures (<1300 bar) because of heterogenization, in exact compliance with the current concepts.

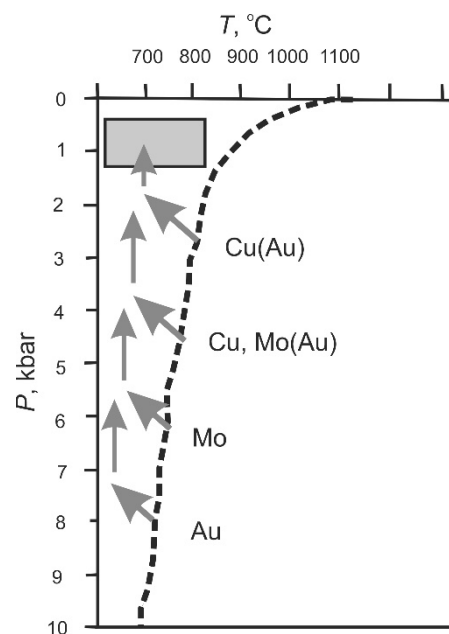


**Figure 11.** Hypothetical dependence of the type of porphyry deposits on the depths at which the mineralizing fluids separated from granitoid magma chamber. Arrows—mineralizing fluids, gray rectangle—area of deposition of ore mineralization. Dotted line—water saturated granite solidus [17].

Of course, this is merely a hypothesis, which calls for test and validation. Other variants are also possible. For example, differences between the fluid compositions can be predetermined by differences between the compositions of the granite melts in the parent magma chambers. However, our hypothesis is able to consistently explain known facts, so it deserves careful tests.

## 5. Conclusions

This article summarizes the currently published data on the composition and parameters of mineralizing fluids of porphyry deposits in the Cu–Mo–Au system. Analysis and comparison of parameters of mineralizing fluids of such porphyry deposits were carried out with the use of boxplots. It was revealed that the highest temperature, salinity, and fluid density are characteristic of Cu(Au)-type deposits, intermediate values of these parameters are observed for Cu, Mo(Au) deposits, and the lowest ones occur for Mo-porphyry and Au-porphyry deposits. Based on the results of this analysis, we propose a scenario according to which mineralizing fluids of different compositions, forming different types of porphyry deposits, are separated from the granitoid melt at different depths.

**Author Contributions:** Conceptualization, V.Y.P.; methodology, V.Y.P. and V.B.N.; software, V.B.N. and V.Y.P.; validation, V.Y.P. and V.B.N.; formal analysis, V.Y.P.; investigation, V.Y.P.; resources, V.B.N.; data curation, V.Y.P.; writing—original draft preparation, V.Y.P. and V.B.N.; writing—review and editing, V.Y.P.; visualization, V.Y.P.; supervision, V.Y.P. and V.B.N.; project administration, V.Y.P.; funding acquisition, V.Y.P. All authors have read and agreed to the published version of the manuscript.

**Funding:** This research was funded by the Russian Science Foundation, project no. 20-17-00184.

**Data Availability Statement:** Not applicable.

**Conflicts of Interest:** The authors declare no conflict of interest.

## References

1. Sillitoe, R.H. A plate tectonic model for the origin of porphyry copper deposits. *Econ. Geol.* **1972**, *67*, 184–197. [[CrossRef](#)]
2. Titley, S.R. Characteristics of porphyry copper occurrence in the American southwest. *Miner. Depos. Modeling. Geol. Assoc. Can. Pap.* **1993**, *40*, 433–464.
3. Seedorf, E.; Dilles, J.H.; Proffett, J.M., Jr.; Einaudi, M.T.; Zurcher, L.; Stavast, W.J.A.; Johnson, D.A.; Barton, M.D. Porphyry Deposits: Characteristics and Origin of Hypogene Features. *Econ. Geol.* **2005**, *100*, 251–298.
4. Sillitoe, R.H. Porphyry copper systems. *Econ. Geol.* **2010**, *105*, 3–41. [[CrossRef](#)]
5. Hedenquist, J.W.; Richards, J.P. The influence of geochemical techniques on the development of genetic models for porphyry copper deposits. *Rev. Econ. Geol.* **1998**, *10*, 235–256.
6. Tosdal, R.M.; Richards, J.P. Magmatic and structural controls on the development of porphyry Cu ± Mo ± Au deposits. *Rev. Econ. Geol.* **2001**, *14*, 157–181.
7. Richards, J.P. Tectonomagmatic precursors for porphyry Cu-(Mo-Au) deposit formation. *Econ. Geol.* **2003**, *98*, 1515–1533. [[CrossRef](#)]
8. Richards, J.P. Magmatic to hydrothermal metal fluxes in convergent and collided margins. *Ore Geol. Rev.* **2011**, *40*, 1–26. [[CrossRef](#)]
9. Cooke, D.R.; Hollings, P.; Walsh, J.L. Giant porphyry deposits: Characteristics, distribution, and tectonic controls. *Econ. Geol.* **2005**, *100*, 801–818. [[CrossRef](#)]
10. Lowell, J.D.; Guilbert, J.M. Lateral and vertical alteration-mineralization zoning in porphyry ore deposits. *Econ. Geol.* **1970**, *65*, 373–408. [[CrossRef](#)]
11. Kirkham, R.V. Intermineral intrusions and their bearing on the origin of porphyry copper and molybdenum deposits. *Econ. Geol.* **1971**, *66*, 1244–1249. [[CrossRef](#)]
12. Beane, R.E.; Titley, S.R. Porphyry copper deposits: Part 2. Hydrothermal alteration and mineralization. *Econ. Geol.* **1981**, *75*, 235–269.
13. Titley, S.R. The style and progress of mineralization and alteration in porphyry copper systems: American Southwest. In *Advances in Geology of the Porphyry Copper Deposits, Southwestern North America*; Titley, S.R., Ed.; University of Arizona Press: Tucson, AZ, USA, 1982; pp. 93–116.
14. Beane, R.E.; Bodnar, R.J. Hydrothermal fluids and hydrothermal alteration in porphyry copper deposits. *Ariz. Geol. Soc. Dig.* **1995**, *20*, 83–93.
15. Gustafson, L.B.; Hunt, J.P. The porphyry copper deposit at El Salvador, Chile. *Econ. Geol.* **1975**, *70*, 857–912. [[CrossRef](#)]
16. Henley, R.W.; McNabb, A. Magmatic vapor plumes and groundwater interaction in porphyry copper emplacement. *Econ. Geol.* **1978**, *73*, 1–20. [[CrossRef](#)]
17. Burnham, C.W. Magmas and hydrothermal fluids. In *Geochemistry of Hydrothermal Ore Deposits*; Barnes, H.L., Ed.; John Wiley & Sons: New York, NY, USA, 1979; pp. 71–136.
18. Burnham, C.W. Magmas and hydrothermal fluids. In *Geochemistry of Hydrothermal Ore Deposits*; Barnes, H.L., Ed.; Wiley and Sons: New York, NY, USA, 1997; pp. 63–123.
19. Holland, H.D. Granites, solutions, and base metal deposits. *Econ. Geol.* **1972**, *67*, 281–301. [[CrossRef](#)]

20. Kilinc, I.A.; Burnham, C.W. Partitioning of chloride between a silicate melt and coexisting aqueous phase from 2 to 8 kilobars. *Econ. Geol.* **1972**, *67*, 231–235. [[CrossRef](#)]
21. Candela, P.A.; Holland, H.D. The partitioning of copper and molybdenum between silicate melts and aqueous fluids. *Geochim. Cosmochim. Acta* **1984**, *48*, 373–380. [[CrossRef](#)]
22. Candela, P.A. Magmatic ore-forming fluids: Thermodynamic and mass-transfer calculations of metal concentrations. In *Ore Deposition Associated With Magmas. Reviews in Economic Geology, 4*; Whitney, J.A., Naldrett, A.J., Eds.; Economic Geology Publishing Company: El Paso, TX, USA, 1989; pp. 203–221.
23. Shinohara, H.; Iiyama, J.T.; Matsuo, S. Partition of chlorine compounds between silicate melt and hydrothermal solutions; I, partition of NaCl-KCl. *Geochim. Cosmochim. Acta* **1989**, *53*, 2617–2630. [[CrossRef](#)]
24. Cline, J.S.; Bodnar, R.J. Can economic porphyry copper mineralization be generated by a typical calc-alkaline melt? *J. Geophys. Res.* **1991**, *96*, 8113–8126. [[CrossRef](#)]
25. Cline, J.S.; Bodnar, R.J. Direct evolution of a brine from crystallizing silicic melt at the Questa, New Mexico, molybdenum deposit. *Econ. Geol.* **1994**, *89*, 1780–1802. [[CrossRef](#)]
26. Bodnar, R.J. Fluid-inclusion evidence for a magmatic source for metals in porphyry copper deposits. *Mineral. Assoc. Can. Short Course Ser.* **1995**, *23*, 139–152.
27. Holtz, F.; Johannes, W.; Tamic, N.; Behrens, H. Maximum and minimum water contents of granitic melts generated in the crust. *Lithos* **2001**, *56*, 1–14. [[CrossRef](#)]
28. Heinrich, C.A.; Driesner, T.; Stefánsson, A.; Seward, T.M. Magmatic vapor concentration and the transport of gold from the porphyry environment to epithermal ore deposits. *Geology* **2004**, *32*, 761–764. [[CrossRef](#)]
29. Rusk, B.; Reed, M.H.; Dilles, J.H.; Klemm, L. Compositions of magmatic-hydrothermal fluids determined by LA-ICPMS of fluid inclusions from the porphyry copper-molybdenum deposit at Butte. *Montana. Chem. Geol.* **2004**, *210*, 173–199. [[CrossRef](#)]
30. Audetat, A.; Pettke, T.; Heinrich, C.A.; Bodnar, R.J. The composition of magmatic-hydrothermal fluids in barren and mineralized intrusions. *Econ. Geol.* **2008**, *103*, 877–908. [[CrossRef](#)]
31. Bodnar, R.J.; Lecumberri-Sanchez, P.; Moncada, D.; Steele-MacInnes, P. *Fluid Inclusions in Hydrothermal Ore Deposits. Reference Module in Earth Systems and Environmental Sciences. Treatise on Geochemistry*, 2nd ed.; Elsevier: Amsterdam, The Netherlands, 2014; pp. 119–142.
32. Driesner, T. The system H<sub>2</sub>O-NaCl. Part II: Correlations for molar volume, enthalpy, and isobaric heat capacity from 0 to 1000 °C, 1 to 5000 bar, and 0 to 1 XNaCl. *Geochim. Cosmochim. Acta* **2007**, *71*, 4902–4919. [[CrossRef](#)]
33. Driesner, T.; Heinrich, C.A. The system H<sub>2</sub>O-NaCl. Part I: Correlation formulae for phase relations in temperature-pressure-composition space from 0 to 1000 °C, 1 to 5000 bar, and 0 to 1 XNaCl. *Geochim. Cosmochim. Acta* **2007**, *71*, 4880–4901. [[CrossRef](#)]
34. Roedder, E. Fluid inclusions: Reviews in Mineralogy. *Mineral. Soc. Am.* **1984**, *12*, 646p.
35. Roedder, E. Fluid inclusions as samples of ore fluids. In *Geochemistry of Hydrothermal Ore Deposits*; Barnes, H.L., Ed.; Holt, Rinehart and Winston: New York, NY, USA, 1967; pp. 515–574.
36. Nash, T.J. Fluid inclusion petrology—Data from porphyry copper deposits and applications to exploration. In *U. S. Geological Survey Professional Paper 907-D*; US Government Printing Office: Washington, DC, USA, 1976; p. 16.
37. Bodnar, R.J. Fluid inclusions in porphyry-type deposits. In *Mineral Deposits Research Review for Industry Course Notes*; The Pennsylvania State University: University Park, PA, USA, 1982; pp. RB1–RB25.
38. Roedder, E.; Bodnar, R.J. Fluid inclusion studies of hydrothermal ore deposits. In *Geochemistry of Hydrothermal Ore Deposits*; Barnes, H.L., Ed.; Wiley & Sons, Inc.: New York, NY, USA, 1997; pp. 657–698.
39. Lecumberri-Sanchez, P.; Newton, M.C.; Westman, E.C.; Kamilli III, R.J.; Canby, V.M.; Bodnar, R.J. Temporal and spatial distribution of alteration, mineralization and fluid inclusion types in the transitional epithermal-porphyry copper system at Red Mountain AZ. *J. Geochem. Explor.* **2013**, *125*, 80–93. [[CrossRef](#)]
40. Becker, S.P.; Bodnar, R.J.; Reynolds, T.J. Temporal and spatial variations in characteristics of fluid inclusions in epizonal magmatic-hydrothermal systems: Applications in exploration for porphyry copper deposits. *J. Geochem. Explor.* **2019**, *204*, 240–255. [[CrossRef](#)]
41. Spooner, E.T.C. Fluid inclusion studies of hydrothermal ore deposits. *Miner. Assoc. Can. Short Course Handb.* **1981**, *6*, 209–240.
42. Weisbrod, A. Fluid inclusions in shallow intrusive. *Miner. Assoc. Can. Short Course Handb.* **1981**, *6*, 241–271.
43. Lattanzi, P. Applications of fluid inclusions in the study and exploration of mineral deposits. *Eur. J. Miner.* **1991**, *3*, 689–701. [[CrossRef](#)]
44. Lattanzi, P. Fluids in ore deposits. In *Fluid inclusions in minerals. Methods and applications*; de Vivo, B., Frezzotti, M.L., Eds.; Virginia Polytechnic Institute and State University, International Mineralogical Association Working Group Short Course: Blacksburg, VA, USA, 1994; pp. 297–307.
45. Wilkinson, J.J. Fluid inclusions in hydrothermal ore deposits. *Lithos* **2001**, *55*, 229–272. [[CrossRef](#)]
46. Kouzmanov, K.; Pokrovski, G.S. Hydrothermal controls on metal distribution in porphyry Cu (-Mo-Au) systems. *Soc. Econ. Geol. Inc. Spec. Publ.* **2012**, *16*, 573–618.
47. Naumov, V.B.; Dorofeeva, V.A.; Mironova, O.F. Physicochemical parameters of the origin of hydrothermal mineral deposits: Evidence from fluid inclusions. IV. Copper and molybdenum. *Geochem. Internat.* **2017**, *55*, 711–725. [[CrossRef](#)]
48. Naumov, V.B.; Dorofeeva, V.A.; Mironova, O.F. Principal physicochemical parameters of natural mineral-forming fluids. *Geochem. Internat.* **2009**, *47*, 777–802. [[CrossRef](#)]

49. Naumov, V.B.; Dorofeeva, V.A.; Mironova, O.F. Physicochemical parameters of the origin of hydrothermal mineral deposits: Evidence from fluid inclusions. VI. Fluorite and barite deposits. *Geochem. Internat.* **2020**, *58*, 1331–1342. [[CrossRef](#)]
50. Kesler, S.E.; Wilkinson, B.H. The role of exhumation in the temporal distribution of ore deposits. *Econ. Geol.* **2006**, *101*, 919–922. [[CrossRef](#)]
51. Roedder, E. Fluid inclusion studies on the porphyry-type ore deposits at Bingham, Utah, Butte, Montana, and Climax, Colorado. *Econ. Geol.* **1971**, *66*, 98–120. [[CrossRef](#)]
52. Nash, J.T.; Theodore, T.G. Ore fluids in the porphyry copper deposit at Copper Canyon, Nevada. *Econ. Geol.* **1971**, *66*, 385–399. [[CrossRef](#)]
53. Berzina, A.P.; Sotnikov, V.I. Some compositional features and parameters of mineral-forming solutions at the Kalmakyr deposit. *Geol. Ore Dep.* **1973**, *4*, 44–50. (In Russian)
54. Moore, W.J.; Nash, J.T. Alteration and fluid inclusion studies of the porphyry copper ore body at Bingham, Utah. *Econ. Geol.* **1974**, *69*, 631–645. [[CrossRef](#)]
55. Chivas, A.R.; Wilkins, R.W.T. Fluid inclusion studies in relation to hydrothermal alteration and mineralization at the Koloula porphyry copper prospect, Guadalcanal. *Econ. Geol.* **1977**, *72*, 153–169. [[CrossRef](#)]
56. Sawkins, F.J. Fluid inclusion studies of the Inguaran copper-bearing breccia pipes, Michaoacan, Mexico. *Econ. Geol.* **1978**, *74*, 924–927. [[CrossRef](#)]
57. Eastoe, C.J. A fluid inclusion study of the Panguna porphyry copper deposit, Bougainville, Papua New Guinea. *Econ. Geol.* **1978**, *73*, 721–748. [[CrossRef](#)]
58. Bodnar, R.J.; Bean, R.E. Temporal and spatial variations in hydrothermal fluid characteristics during vein filling in preore cover overlying deeply Buried porphyry copper-type mineralization at Red Mountain, Arizona. *Econ. Geol.* **1980**, *75*, 875–893. [[CrossRef](#)]
59. Preece, R.K., III; Bean, R.E. Contrasting evolutions of hydrothermal alteration in quartz monzonite and quartz diorite wall rocks at the Sierrita porphyry copper deposit, Arizona. *Econ. Geol.* **1982**, *77*, 1621–1641. [[CrossRef](#)]
60. Simmons, S.F.; Sawkins, F.J. Mineralogic and fluid inclusion studies of the Washington Cu-Mo-W-bearing breccia pipe, Sonora, Mexico. *Econ. Geol.* **1983**, *78*, 521–526. [[CrossRef](#)]
61. Shelton, K.L. Composition and origin of ore-forming fluids in a carbonate-hosted porphyry copper and skarn deposit: A fluid inclusion and stable isotope study of Mines Gaspé, Quebec. *Econ. Geol.* **1983**, *78*, 387–421. [[CrossRef](#)]
62. Reynolds, T.J.; Beane, R.E. Evolution of hydrothermal fluid characteristics at the Santa Rita, New Mexico, porphyry copper deposit. *Econ. Geol.* **1985**, *80*, 1328–1347. [[CrossRef](#)]
63. Scherkenbach, D.A.; Sawkins, F.J.; Sayfried, W.E., Jr. Geologic, fluid inclusion, and geochemical studies of the mineralized breccias at Cumobabi, Sonora, Mexico. *Econ. Geol.* **1985**, *80*, 1566–1592. [[CrossRef](#)]
64. Lang, J.R.; Eastoe, C.J. Relationships between a porphyry Cu-Mo deposit, base and precious metal veins, and Laramide intrusions, Mineral Park, Arizona. *Econ. Geol.* **1988**, *83*, 551–567. [[CrossRef](#)]
65. Anderson, A.J.; Clark, A.H.; Ma, X.-P.; Palmer, G.R.; MacArthur, D.; Roedder, E. Proton-induced X-Ray and Gamma-Ray emission analysis of unopened fluid inclusions. *Econ. Geol.* **1989**, *84*, 924–939. [[CrossRef](#)]
66. John, D.A. Evolution of hydrothermal fluids in the Park Premier Stock, Central Wasatch Mountains, Utah. *Econ. Geol.* **1989**, *84*, 879–902. [[CrossRef](#)]
67. Hezarkhani, A.; Williams-Jones, A.E. Controls of alteration and mineralization in the Sungun porphyry copper deposit, Iran: Evidence from fluid inclusions and stable isotopes. *Econ. Geol.* **1998**, *93*, 651–670. [[CrossRef](#)]
68. Hedenquist, J.W.; Arribas, A.J.; Reynolds, T.J. Evolution of an Intrusion-Centered Hydrothermal System: Far Southeast-Lepanto Porphyry and Epithermal Cu-Au Deposits, Philippines. *Econ. Geol.* **1998**, *93*, 373–404. [[CrossRef](#)]
69. Ulrich, T.; Günther, D.; Heinrich, C.A. Gold concentrations of magmatic brines and the metal budget of porphyry copper deposits. *Nature* **1999**, *399*, 676–679. [[CrossRef](#)]
70. Rombach, C.S.; Newberry, R.J. Shotgun deposit: Granite porphyry-hosted gold-arsenic mineralization in southwestern Alaska, USA. *Mineral. Depos.* **2001**, *36*, 607–621. [[CrossRef](#)]
71. Vanko, D.A.; Bonnin-Mosbah, M.; Philippot, P.; Roedder, E.; Sutton, S.R. Fluid inclusions in quartz from oceanic hydrothermal specimens and the Bingham, Utah porphyry-Cu deposit: A study with PIXE and SXRF. *Chem. Geol.* **2001**, *173*, 227–238. [[CrossRef](#)]
72. Ulrich, T.; Gunther, D.; Heinrich, C.A. The evolution of a porphyry Cu-Au deposit, based on LA-ICP-MS analysis of fluid inclusions: Bajo de la Alumbrera, Argentina. *Econ. Geol.* **2002**, *97*, 1889–1920. [[CrossRef](#)]
73. Audétat, A.; Pettke, T. The magmatic-hydrothermal evolution of two barren granites: A melt and fluid inclusion study of the Rito del Medio and Cañada Pinabete plutons in northern New Mexico (USA). *Geochim. Cosmochim. Acta* **2003**, *67*, 97–121. [[CrossRef](#)]
74. Harris, A.C.; Kamenetsky, V.S.; White, N.C.; van Achterbergh, E.; Ryan, C.G. Melt inclusions in veins: Linking magmas and porphyry Cu deposits. *Science* **2003**, *302*, 2109–2111. [[CrossRef](#)]
75. Padilla-Garza, R.A.; Titley, S.R.; Eastoe, C.J. Hypogene evolution of the Escondida porphyry copper deposit, Chile. *Econ. Geol. Spec. Publ.* **2004**, *11*, 141–165.
76. Harris, A.C.; Kamenetsky, V.S.; White, N.C.; Steele, D.A. Volatile phase separation in silicic magmas at Bajo de la Alumbrera porphyry Cu-Au deposit, NW Argentina. *Resour. Geol.* **2004**, *54*, 341–356. [[CrossRef](#)]

77. Landtwing, M.R.; Pettke, T.; Halter, W.E.; Heinrich, C.A.; Redmond, P.B.; Einaudi, M.T.; Kunze, K. Copper deposition during quartz dissolution by cooling magmatic–hydrothermal fluids: The Bingham porphyry. *Earth Planet. Sci. Lett.* **2005**, *235*, 229–243. [[CrossRef](#)]
78. Davidson, P.; Kamenetsky, V.; Cook, D.R.; Friksen, P.; Hollings, P.; Ryan, C.; Achtenbergh, E.V.; Mernagh, T.; Scarmeta, J.; Serrano, L.; et al. Magmatic precursors of hydrothermal fluids at the Río Blanco Cu-Mo deposit, Chile: Links to silicate magmas and metal transport. *Econ. Geol.* **2005**, *100*, 963–978. [[CrossRef](#)]
79. Masterman, G.J.; Cooke, D.R.; Berry, R.F.; Walshe, J.L.; Lee, A.W.; Clark, A.H. Fluid chemistry, structural setting, and emplacement history of the Rosario Cu-Mo porphyry and Cu-Ag-Au epithermal veins, Collahuasi district, Northern Chile. *Econ. Geol.* **2005**, *100*, 835–862. [[CrossRef](#)]
80. Bouzari, F.; Clark, A.H. Prograde evolution and geothermal affinities of a major porphyry copper deposit: The Cerro Colorado hypogene protore, I Región, Northern Chile. *Econ. Geol.* **2006**, *101*, 95–134. [[CrossRef](#)]
81. Klemm, L.M.; Pettke, T.; Heinrich, C.A.; Campos, E. Hydrothermal evolution of the El Teniente deposit, Chile: Porphyry Cu-Mo ore deposition from low-salinity magmatic fluids. *Econ. Geol.* **2007**, *102*, 1021–1045. [[CrossRef](#)]
82. Kovalenkev, V.A.; Krylova, T.L.; Kiseleva, G.D.; Kigai, I.N. Parameters of processes that produced the atypical Bugdainskoe Au-Mo(W)-Pb-Zn porphyry deposit, eastern Transbaikalia, Russia. *Dokl. Acad. Sci. Rus.* **2007**, *416*, 96–99. (In Russian)
83. Lai, J.; Chi, G.; Peng, S.; Shao, Y.; Yang, B. Fluid evolution in the formation of the Fenghuangshan Cu-Fe-Au deposit, Tongling, Anhui, China. *Econ. Geol.* **2007**, *102*, 949–970. [[CrossRef](#)]
84. Prokofiev, V.Y.; Zorina, L.D.; Kovalenker, V.A.; Akinfiyev, N.N.; Baksheev, I.A.; Krasnov, A.N.; Yurgenson, G.A.; Trubkin, N.V. Composition, Formation Conditions, and Genesis of the Talatui Gold Deposit, the Eastern Transbaikalian Region, Russia. *Geol. Ore Depos.* **2007**, *49*, 31–68. [[CrossRef](#)]
85. Rusk, B.G.; Reed, M.H.; Dilles, J.H. Fluid inclusion evidence for magmatic-hydrothermal fluid evolution in the porphyry copper-molybdenum deposit at Butte, Montana. *Econ. Geol.* **2008**, *103*, 307–334. [[CrossRef](#)]
86. Valencia, V.A.; Eastoe, C.; Ruiz, J.; Ochoa-Landin, L.; Gehrels, G.; Gonzalez-Lion, C.; Barra, F.; Espinoza, E. Hydrothermal evolution of the porphyry copper deposit at La Caridad, Sonora, Mexico, and the relationship with a neighboring high-sulfidation epithermal deposit. *Econ. Geol.* **2008**, *103*, 475–491. [[CrossRef](#)]
87. Klemm, L.M.; Pettke, T.; Heinrich, C.A. Fluid and source magma evolution of the Questa porphyry Mo deposit, New Mexico, USA. *Mineral. Depos.* **2008**, *43*, 533–552. [[CrossRef](#)]
88. Pudack, C.; Halter, W.E.; Heinrich, C.A.; Pettke, T. Evolution of magmatic vapor to gold-rich epithermal liquid: The porphyry to epithermal transition at Nevados de Famatina, Northwest Argentina. *Econ. Geol.* **2009**, *104*, 449–477. [[CrossRef](#)]
89. Xu, W.Y.; Pan, F.C.; Qu, X.M.; Hou, Z.Q.; Yang, Z.S.; Chen, W.S.; Yang, D.; Cui, Y. Xiongcu, Tibet: A telescoped system of veinlet-disseminated Cu (Au) mineralization and late vein-style Au (Ag)-polymetallic mineralization in a continental collision zone. *Ore Geol. Rev.* **2009**, *36*, 174–193. [[CrossRef](#)]
90. Chen, Y.J.; Pirajno, F.; Li, N.; Guo, D.S.; Lai, Y. Isotope systematics and fluid inclusion studies of the Qiyugou breccia pipe-hosted gold deposit, Qinling Orogen, Henan province, China: Implications for ore genesis. *Ore Geol. Rev.* **2009**, *35*, 245–261. [[CrossRef](#)]
91. Seo, J.H.; Guillong, M.; Heinrich, C.A. The role of sulfur in the formation of magmatic-hydrothermal copper-gold deposits. *Earth Planet. Sci. Lett.* **2009**, *282*, 323–328. [[CrossRef](#)]
92. Landtwing, M.R.; Furrer, C.; Redmond, P.B.; Pettke, T.; Guillong, M.; Heinrich, C.A. The Bingham Canyon Porphyry Cu-Mo-Au Deposit. III. Zoned Copper-Gold Ore Deposition by Magmatic Vapor Expansion. *Econ. Geol.* **2010**, *105*, 91–118. [[CrossRef](#)]
93. Shen, P.; Shen, Y.C.; Wang, J.B.; Zhu, H.P.; Wang, L.J.; Meng, L. Methane-rich fluid evolution of the Baogutu porphyry Cu-Mo-Au deposit, Xinjiang, NW China. *Chem. Geol.* **2010**, *275*, 78–98. [[CrossRef](#)]
94. Fan, H.R.; Hu, F.F.; Wilde, S.A.; Yang, K.F.; Jin, C.W. The Qiyugou gold-bearing breccia pipes, Xiong'er shan region, central China: Fluid-inclusion and stable-isotope evidence for an origin from magmatic fluids. *Intern. Geol. Rev.* **2011**, *53*, 25–45. [[CrossRef](#)]
95. Deng, J.; Wang, Q.F.; Xiao, C.H.; Yang, L.Q.; Liu, H.; Gong, Q.G.; Zhang, J. Tectonic-magmatic-metallogenic system, Tongling ore cluster region, Anhui Province, China. *Intern. Geol. Rev.* **2011**, *53*, 449–476. [[CrossRef](#)]
96. Gu, L.X.; Wu, C.Z.; Zhang, Z.Z.; Pirajno, F.; Ni, P.; Chen, P.R.; Xiao, X.J. Comparative study of ore-forming fluids of hydrothermal copper-gold deposits in the lower Yangtze River Valley, China. *Intern. Geol. Rev.* **2011**, *53*, 477–498. [[CrossRef](#)]
97. Xu, X.C.; Zhang, Z.Z.; Liu, Q.N.; Lou, J.W.; Xie, Q.Q.; Chu, P.L.; Frost, R.L. Thermodynamic study of the association and separation of copper and gold in the Shizishan ore field, Tongling, Anhui Province, China. *Ore Geol. Rev.* **2011**, *43*, 347–358. [[CrossRef](#)]
98. Li, J.X.; Li, G.M.; Qin, K.Z.; Xiao, B. High-temperature magmatic fluid exsolved from magma at the Duobuza porphyry copper-gold deposit, Northern Tibet. *Geofluids* **2011**, *11*, 134–143. [[CrossRef](#)]
99. Allan, M.M.; Morrison, G.W.; Yardley, B.W.D. Physicochemical evolution of a porphyry-breccia system: A laser ablation ICP-MS study of fluid inclusions in the Mount Leyshon Au deposit, Queensland, Australia. *Econ. Geol.* **2011**, *106*, 413–436. [[CrossRef](#)]
100. Wolf, R.C.; Cooke, D.R. Geology of the Didipio region and genesis of the Dinkidi alkalic porphyry Cu-Au deposit and related pegmatites, northern Luzon, Philippines. *Econ. Geol.* **2011**, *106*, 1279–1315. [[CrossRef](#)]
101. Seo, J.H.; Guillong, M.; Heinrich, C.A. Separation of molybdenum and copper in porphyry deposits: The roles of sulfur, redox, and pH in ore mineral deposition at Bingham Canyon. *Econ. Geol.* **2012**, *107*, 333–356. [[CrossRef](#)]
102. Soloviev, S.G.; Kryazhev, S.G.; Dvurechenskaya, S.S. Geology, mineralization, stable isotope geochemistry, and fluid inclusion characteristics of the Novogodnee-Monto oxidized Au-(Cu) skarn and porphyry deposit, Polar Ural, Russia. *Mineral. Depos.* **2013**, *48*, 603–627. [[CrossRef](#)]

103. Koděra, P.; Heinrich, C.A.; Wälle, M.; Lexa, J. Magmatic salt melt and vapor: Extreme fluids forming porphyry gold deposits in shallow subvolcanic settings. *Geology* **2014**, *42*, 495–498. [[CrossRef](#)]
104. Zhang, H.D.; Zhang, H.-F.; Santosh, M.; Li, S.R. Fluid inclusions from the Jinchang Cu–Au deposit, Heilongjiang Province, NE China: Genetic style and magmatic-hydrothermal evolution. *J. Asian Earth Sci.* **2014**, *82*, 103–114. [[CrossRef](#)]
105. Siahcheshm, K.; Calagari, A.A.; Abedini, A. Hydrothermal evolution in the Maher-Abad porphyry Cu–Au deposit, SW Birjand, Eastern Iran: Evidence from fluid inclusions. *Ore Geol. Rev.* **2014**, *58*, 1–13. [[CrossRef](#)]
106. Nikolaev, Y.N.; Prokof'ev, V.Y.; Baksheev, I.A.; Chitalin, A.F.; Marushchenko, L.I.; Kal'ko, I.A. The First Data on the Zoned Distribution of Fluid Inclusions in the Ore-Forming System of the Peschanka Gold-Copper-Porphyry Deposit (Northeast Russia). *Dokl. Earth Sci.* **2014**, *459*, 1615–1618. [[CrossRef](#)]
107. Simmonds, V.; Calagari, A.A.; Kyser, K. Fluid inclusion and stable isotope studies of the Kighal porphyry Cu–Mo prospect, East-Azerbaijan, NW Iran. *Arab. J. Geosci.* **2015**, *8*, 437–453. [[CrossRef](#)]
108. Audetat, A. Compositional evolution and formation conditions of magmas and fluids related to porphyry Mo mineralization at Climax, Colorado. *J. Petrol.* **2015**, *56*, 1519–1546. [[CrossRef](#)]
109. Nikolaev, Y.N.; Baksheev, I.A.; Prokofiev, V.Y.; Nagornaya, E.V.; Marushchenko, L.I.; Sidorina, Y.N.; Chitalin, A.F.; Kal'ko, I.A. Gold–Silver Mineralization in Porphyry–Epithermal Systems of the Baimka Trend, Western Chukchi Peninsula, Russia. *Geol. Ore Depos.* **2016**, *58*, 319–345. [[CrossRef](#)]
110. Liu, X.; Fan, H.R.; Hu, F.F.; Yang, K.F.; Wen, B.J. Nature and evolution of the ore-forming fluids in the giant Dexing porphyry Cu–Mo–Au deposit, Southeastern China. *J. Geochem. Explor.* **2016**, *171*, 83–95. [[CrossRef](#)]
111. Khomenko, M.O.; Giebsher, N.A.; Tomilenko, A.A.; Bul'bak, T.A.; Ryabukha, M.A.; Semenova, D.V. Physicochemical parameters and age of the Vasil'kovskoe gold deposit (northern Kazakhstan). *Russ. Geol. Geophys.* **2016**, *57*, 1728–1744. [[CrossRef](#)]
112. Bukhanova, D.S.; Plechov, P.Y. Parameters of processes that produced the Malmyzhskoe Au–Cu porphyry deposit: Evidence from fluid inclusions. *Her. KRAUNTS* **2017**, *34*, 61–71. (In Russian)
113. Gregory, M.J. A fluid inclusion and stable isotope study of the Pebble porphyry copper-gold-molybdenum deposit, Alaska. *Ore Geol. Rev.* **2017**, *80*, 1279–1303. [[CrossRef](#)]
114. Kouhestani, H.; Mokhtari, M.A.A.; Chang, Z.; Stein, H.J.; Johnson, C.A. Timing and genesis of ore formation in the Qarachilar Cu–Mo–Au deposit, Ahar–Arasbaran metallogenic zone, NW Iran: Evidence from geology, fluid inclusions, O–S isotopes and Re–Os geochronology. *Ore Geol. Rev.* **2018**, *102*, 757–775. [[CrossRef](#)]
115. Wang, D.; Bi, X.; Lu, H.; Hu, R.; Wang, X.; Xu, L. Fluid and melt inclusion study on mineralized and barren porphyries, Jinshajiang–Red River alkali-rich intrusive belt, and significance to metallogenesis. *J. Geochem. Explor.* **2018**, *184*, 28–39. [[CrossRef](#)]
116. Zhang, W.; Williams-Jones, A.E.; Leng, C.-B.; Zhang, X.-C.; Chen, W.T.; Qin, C.-J.; Su, W.-C.; Yan, J.-H. The origin of CH<sub>4</sub>-rich fluids in reduced porphyry–skarn Cu–Mo–Au systems. *Ore Geol. Rev.* **2019**, *114*, 103135. [[CrossRef](#)]
117. Soloviev, S.G.; Kryazhev, S.G.; Dvurechenskay, S.S.; Vasyukov, V.E.; Shumilin, D.A.; Voskresensky, K.I. The superlarge Malmyzh porphyry Cu–Au deposit, Sikhote-Alin, eastern Russia: Igneous geochemistry, hydrothermal alteration, mineralization, and fluid inclusion characteristics. *Ore Geol. Rev.* **2019**, *113*, 103112. [[CrossRef](#)]
118. Mernagh, T.; Mavrogenes, J. Significance of high temperature fluids and melts in the Grasberg porphyry copper gold deposit. *Chem. Geol.* **2019**, *508*, 210–224. [[CrossRef](#)]
119. Lang, X.; Deng, Y.; Wang, X.; Tang, J.; Xie, F.; Yang, Z.; Yin, Q.; Jiang, K. Reduced fluids in porphyry copper-gold systems reflect the occurrence of the wall-rock thermogenic process: An example from the No.1 deposit in the Xiongqun district, Tibet, China. *Ore Geol. Rev.* **2020**, *118*, 103212. [[CrossRef](#)]
120. Haniłci, N.; Bozkaya, G.; Banks, D.A.; Bozkaya, O.; Prokofiev, V.; Öztaş, Y. Fluid inclusion characteristics of the Kışladağ porphyry Au deposit, Western Turkey. *Minerals* **2020**, *10*, 64. [[CrossRef](#)]
121. Mernagh, T.; Leys, C.; Henley, R.W. Fluid inclusion systematics in porphyry copper deposits: The super-giant Grasberg deposit, Indonesia, as a case study. *Ore Geol. Rev.* **2020**, *123*, 103570. [[CrossRef](#)]
122. Chen, P.; Zeng, Q.; Zhou, L.; Zhou, T. Fluid inclusion evidence for hydrothermal evolution of the Sadaigoumen porphyry Mo deposit on the northern margin of the north China Craton. *Ore Geol. Rev.* **2021**, *134*, 104145. [[CrossRef](#)]
123. Brown, P.E. Flincor: A microcomputer program for the reduction and investigation of fluid inclusion data. *Am. Mineral.* **1989**, *74*, 1390–1393.
124. Koděra, P.; Tacách, Á.; Racek, M.; Šimko, F.; Luptáková, I.; Váci, T.; Antal, P. Javorieite, KFeCl<sub>3</sub>: A new mineral hosted by salt melt inclusions in porphyry gold systems. *Eur. J. Mineral.* **2017**, *6*, 995–1004. [[CrossRef](#)]
125. Pintea, I.; Udubaşa, S.S.; Latan, E.L.; Berbelec, I.; Bîrgăoanu, D.; Ciobotea-Barbu, O.C.; Ghinescu, E. Microthermometry and Raman spectroscopy of fluid and melt inclusions in the alpine porphyry copper deposits from Romania: Insights on micrometallogeny. *Rom. J. Miner. Depos.* **2019**, *92*, 9–32.
126. Roedder, E.; Skinner, B.J. Experimental evidence that fluid inclusions do not leak. *Econ. Geol.* **1968**, *63*, 715–730. [[CrossRef](#)]
127. Mavrogenes, J.A.; Bodnar, R.J. Hydrogen movement into and out of fluid inclusions in quartz: Experimental evidence and geologic implications. *Geochim. Cosmochim. Acta* **1994**, *58*, 141–148. [[CrossRef](#)]